

This is a non-peer reviewed pre-print submitted to EarthArxiv.  
Subsequent peer-reviewed versions of this manuscript may have slightly different content. The authors welcome feedback.

Please contact Sandy H. S. Herho ([sandy.herho@email.ucr.edu](mailto:sandy.herho@email.ucr.edu)) regarding this manuscript's content.

# imc-precip-iso: Open monthly stable isotope data of precipitation over the Indonesian Maritime Continent

R. Suwarman<sup>1</sup>, S. H. S. Herho<sup>2,3,\*</sup>, H. A. Belgaman<sup>4</sup>, D. E. Irawan<sup>5</sup>, K. Ichiyanagi<sup>6</sup>, I. M. Yosa<sup>1</sup>, A. I. D. Utami<sup>7</sup>, S. Prayogo<sup>8</sup>, and E. Aldrian<sup>4</sup>

<sup>1</sup>Atmospheric Science Research Group, Bandung Institute of Technology (ITB), Bandung, Indonesia

<sup>2</sup>Department of Earth and Planetary Sciences, University of California, Riverside, USA

<sup>3</sup>Department of Geology, University of Maryland, College Park, USA

<sup>4</sup>Research Center for Climate and Atmosphere (PRIMA), National Research and Innovation Agency (BRIN), Bandung, Indonesia

<sup>5</sup>Applied Geology Research Group, Bandung Institute of Technology (ITB), Bandung, Indonesia

<sup>6</sup>Faculty of Advanced Science and Technology, Kumamoto University, Kumamoto, Japan

<sup>7</sup>Indonesian Meteorology, Climatology, and Geophysical Agency (BMKG), Jakarta, Indonesia

<sup>8</sup>Software Engineering Division, Manvis Teknologi Engineering, Bandung, Indonesia

\*Corresponding author: [sandy.herho@email.ucr.edu](mailto:sandy.herho@email.ucr.edu)

## Abstract

Stable isotopes,  $\delta^2\text{H}$ ,  $\delta^{18}\text{O}$ , and d-excess, are valuable tools as natural tracers of diffusion processes and phase changes in the global hydroclimatological cycle. The Indonesian Maritime Continent (IMC) is an archipelago area surrounded by very warm waters which induce convective activities as the primary heat source driving global atmospheric circulation. Given the central role of IMC in this hydroclimatological cycle, comprehensive study and data collection on the stable isotopes of precipitation in this region is crucial.

In this study, we collected monthly stable isotope data from 62 stations spread throughout the Indonesian archipelago from September 2010 to September 2017. We cleaned the data and conducted quality control activities by comparing the Local Meteoric Water Line (LMWL) to previous studies in a similar climatic region. We shared these data openly on our GitHub repository, making them easier to update and interact with users in the future.

## 1 Introduction

Indonesian Maritime Continent (IMC) comprises a group of islands surrounded by the Indian and Pacific Oceans. The region's climate is influenced by its insular geography and its position near the Equator. Located in the western part of the Indo-Pacific warm pool (IPWP), IMC is a source of latent heat release and deep convection which drives the Hadley and Walker cells, thus playing an essential role in the earth's hydrological cycle (1; 2). IMC is also the only link for warmed surface waters from the Pacific Ocean to the Indian Ocean through the Indonesian Throughflow (ITF), a surface flow component of the global ocean conveyor belt (e. g. 3; 4; 5; 6; 7).

In general, IMC experiences two seasons, namely the wet and dry seasons, each in boreal winter - spring (November-March/NDJFM) and boreal summer - fall (May - September/MJJAS) (8; 1). During the wet season, there is warm sea surface temperature (SST) and heavy precipitation over the IMC, which is brought by the Asian winter monsoon, which is northeasterly to the north of the equator and northwesterly to the south of the equator, the opposite also happens in the dry season (9; 10; 1). Besides the annual cycle, IMC precipitation is influenced by internal global atmosphere-ocean interactions, such as the El Niño Southern Oscillation (ENSO) (e. g. 11; 12; 13; 14; 15) and the Indian Ocean Dipole mode (IOD) (e. g. 1; 16; 11; 17). On an

45 intra-annual scale, precipitation over the IMC is also influenced by the Madden-Julian Oscillation (MJO),  
46 which propagates from the Indian Ocean to the Pacific Ocean via IMC (e. g. 18; 19; 11; 20; 21; 22).

47 Given the importance of IMC in understanding the earth's hydroclimatological phenomena (23), investiga-  
48 tion of precipitation characteristics is inevitable. One of the characteristics of precipitation that is important  
49 to investigate is the traditional water-stable isotopes of precipitation ( $\delta^{18}\text{O}$  and  $\delta^2\text{H}$ ) which are considered  
50 one of the natural tracers of hydrological cycles as a consequence of equilibrium and kinetic processes dur-  
51 ing phase transitions and diffusive processes (24; 25; 26; 27). In general, oxygen-18 ( $\delta^{18}\text{O}$ ) and deuterium  
52 ( $\delta^2\text{H}$ ) at mid- and high-latitudes are correlated with temperature (e. g. 28; 29; 30; 31; 32). However, in tropi-  
53 cal regions such as the IMC, these two isotopic compositions show a negative correlation (e.g. 33; 34; 35; 36)  
54 due to a rainout process known as the amount effect (37).  $\delta^{18}\text{O}$  can also be used as a signature of the wa-  
55 ter vapour transport process during ENSO and MJO over the IMC (38; 39; 40). Observations of  $\delta^{18}\text{O}$  and  
56  $\delta^2\text{H}$  in the tropics are also crucial to confirm the sensitivity of proxy precipitation observations in paleo-  
57 climatology using proxy system modelling (PSM), which requires modern precipitation isotope data in the  
58 region (41). Modern precipitation isotope observations are also needed to correct calculations performed  
59 by isotope-enabled General Circulation Models (iGCMs) (e. g. 42; 43; 44; 45).

60 Until recently, there is not much open and publicly accessible data on traditional precipitation isotope  
61 over the IMC. There are four isotope stations operated by the International Atomic Energy Agency (IAEA)  
62 within the framework of the Global Network of Isotopes in Precipitation (GNIP) program. However, these  
63 stations stopped operating in 2003 and only cover the Java region, except for the Jayapura station in Papua  
64 (46). In addition, there were isotope observations conducted by the Institute of Observational Research  
65 for Global Change (IORGC)/Japan Agency for Marine-Earth Science and Technology (JAMSTEC) conducted  
66 at six stations across IMC between 2001 and 2007 (33; 46).

67 In this study, we conducted monthly  $\delta^{18}\text{O}$  and  $\delta^2\text{H}$  sampling at 62 observation stations along the IMC  
68 from September 2010 to September 2017. Part of these data (30 stations) have been used in a study by  
69 Belgaman et al. (47) but has yet to be opened to the public. We opened the  $\delta^{18}\text{O}$  and  $\delta^2\text{H}$  measurements  
70 to the public on our GitHub repository to support democratizing knowledge based on open-source code  
71 and reproducible datasets (48).

## 72 2 Material and Methods

### 73 2.1 Data Acquisition

74 We conducted field sampling from 62 meteorological and climatological stations owned by the Indonesian  
75 Meteorology, Climatology, and Geophysical Agency (BMKG) throughout the IMC area (Figure 1). To find out  
76 the details of station numbering and their location, see the table on the following URL: [https://github.com/sandyherho/imc-precip-iso/blob/main/output\\_data/sta\\_list.csv](https://github.com/sandyherho/imc-precip-iso/blob/main/output_data/sta_list.csv). We collected these pre-  
77 cipitation samples manually using buckets and then put them into 6 mL glass vials with screw caps. We  
78 collected this monthly precipitation samples from September 2010 to September 2017.

80 We measured  $\delta^{18}\text{O}$  and  $\delta^2\text{H}$  using the Picarro<sup>®</sup> L2120-i instrument using the cavity ring-down spectroscopy  
81 technique, which has proven practical and accurate in measuring water isotopes (e. g. 51; 52; 53; 54; 55).  
82 We measured the ratio of the abundance of the heavy to light isotopes ( $R$ ), in the context of this study,  
83  $^2\text{H}/^1\text{H}$  and  $^{18}\text{O}/^{16}\text{O}$ , from samples by comparing them to the international standard, namely the Vienna  
84 Standard Mean Ocean Water (VSMOW) (56) so that  $\delta$  values were obtained in units per mil (‰) using the  
85 following equation:

$$\delta = \left( \frac{R_{\text{sample}}}{R_{\text{standard}}} - 1 \right) \times 10^3 \quad (1)$$

86 Due to the limited supply of international standards ( $is$ ), we calibrated the samples ( $x$ ) using three working  
87 standards ( $ws$ ), Aqua Standard<sup>®</sup>, SLW2 and ICE2, which had been calibrated against VSMOW. This calcula-  
88 tion process is formulated through the following equation (57):

$$\delta_{x-is} = \delta_{x-ws} + \delta_{ws-is} + (\delta_{x-ws} \times \delta_{ws-is}) \times 10^{-3} \quad (2)$$

89 Long-term standard errors ( $1\sigma$ ) for these  $\delta^{18}\text{O}$  and  $\delta^2\text{H}$  measurements are  $\pm 0.08$  ‰ and  $\pm 0.22$  ‰, re-  
90 spectively (47).

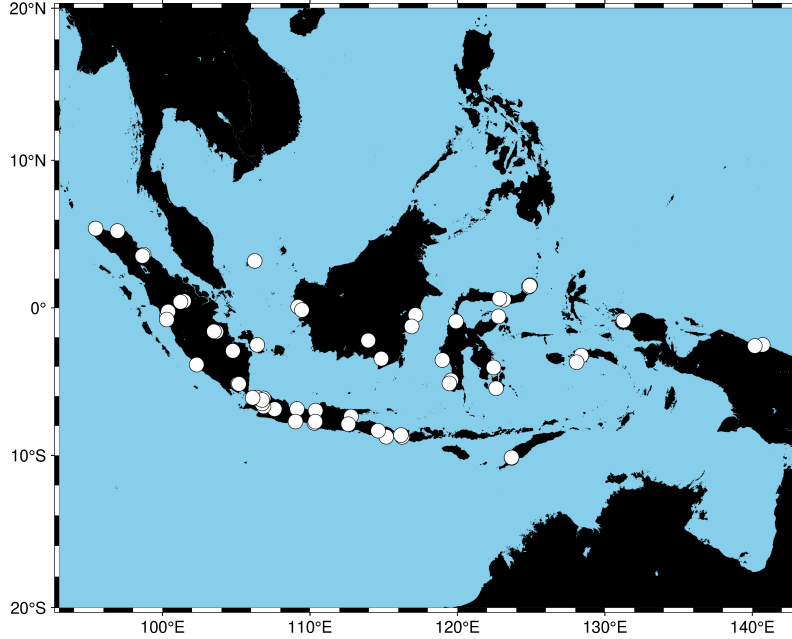


Figure 1: Location of the stations at which monthly samples of precipitation were collected for isotope measurements over the IMC (rendered using PyGMT (49; 50)).

## 91 2.2 Data Wrangling

92 Microsoft® Excel files extracted from the isotope measurement instrument were then converted into a text-  
 93 formatted files, i. e. comma-separated values (CSV) format to make them easier to read by various kinds  
 94 of software without being limited by a paid license (58; 59). These data were then splitted into time series  
 95 for each station and the entire IMC. In addition, we also calculated d-excess ( $d$ ), which is defined as the  
 96 deviation from  $\delta^2\text{H}$  to  $\delta^{18}\text{O}$  according to the definition of the Global Meteoric Water Line (GMWL) (60),  
 97 which can be written as follows:

$$d = \delta^2\text{H} - 8\delta^{18}\text{O} \quad (3)$$

98 Calculation of this d-excess is necessary, given its correlation with the oceanic source of precipitation  
 99 (61; 28). Globally, this d-excess is a dependent variable of the relative humidity of the sea surface (62).  
 100 Using d-excess, we can find the moisture flux anomaly during extreme events, such as ENSO influences in  
 101 precipitation (e. g. 63; 64; 65). We did the entire data wrangling process using NumPy (66) and pandas  
 102 (67) libraries in the Python computing environment.

## 103 2.3 Local Meteoric Water Line (LMWL) Estimation

104 We performed Local Meteoric Water Line (LMWL) calculations as part of our quality control efforts. It has  
 105 been known since a study conducted by Craig (60) that there is a linear relationship between  $\delta^2\text{H}$  to  $\delta^{18}\text{O}$   
 106 globally, which can be formulated as follows:

$$\delta^2\text{H} = 8\delta^{18}\text{O} + 10 \quad (4)$$

107 However, local slope variations and intercepts were only discovered after collecting IAEA/GNIP observa-  
 108 tions through the study of Rozanski et al. (68), better known as LMWL. In this study, it is emphasized that  
 109 the relationship between the two isotopes is still linear. Variations in the slope may store information about  
 110 the local seasonal climatology (69).

111 We used Bayesian Linear Regression (BLR) to determine the relationship between  $\delta^2\text{H}$  and  $\delta^{18}\text{O}$  over the  
 112 IMC. BLR allows better handling of uncertainty in models. This method recognizes that we need perfect  
 113 information about model parameters or data variability. We can represent this uncertainty using a proba-  
 114 bility distribution on the parameters in the Bayesian approach. This approach helps generate more realistic  
 115 and credible parameter estimates and confidence intervals. The BLR approach allows us to incorporate any

116 prior knowledge about the model parameters. This is useful when we need more data or want to use ex-  
 117 isting domain knowledge. In this study, we determined the priors for slopes and intercepts from the global  
 118 data compilation for humid tropical regions (Köppen class A) that was done by Putman et al. (69). Apart  
 119 from single-point estimates (as in "frequentist" linear regression), the BLR gives a full posterior distribu-  
 120 tion of model parameters after looking at the data. This provides richer information about the parameter  
 121 uncertainties and allows for more robust modelling of the  $\delta^2\text{H} - \delta^{18}\text{O}$  covariance. Because of these ad-  
 122 vantages, the Bayesian approaches have recently been popular for solving water isotope problems (e. g.  
 123 69; 70; 71; 72; 73; 74; 75). The full benefits of using BLR can be found in Klauenberg et al. (76).

124 The simple linear regression model that we used to explain the statistical relationship between  $\delta^2\text{H}$  and  
 125  $\delta^{18}\text{O}$  is illustrated in the following equation:

$$\delta^2\text{H}_i = \beta_0 + \beta_1\delta^{18}\text{O}_i + \varepsilon_i \quad (5)$$

126 , where  $\delta^2\text{H}_i$  and  $\delta^{18}\text{O}_i$  are the observed deuterium and oxygen-18 isotope values for the  $i$ -th data point,  
 127 respectively.  $\beta_0$  and  $\beta_1$  are the unknown regression coefficients (intercept and slope) to be estimated.  
 128  $\varepsilon_i$  is the random error term, assumed to be normally distributed, with mean zero and constant variance  
 129  $\sigma^2$ .

130 BLR estimation started by specifying the prior distributions for the unknown parameters:  $\beta_0$ ,  $\beta_1$ , and  $\sigma^2$ .  
 131 In this study, we assumed normal prior for intercept and slope, and uniform prior for variance (77):

$$\begin{cases} \beta_0 \sim \mathcal{N}(m_0, s_0^2) \\ \beta_1 \sim \mathcal{N}(m_1, s_1^2) \\ \sigma^2 \sim U(a, b) \end{cases} \quad (6)$$

132 Parameters  $m_0$ ,  $m_1$ ,  $s_0$ ,  $s_1$ ,  $a$ , and  $b$  were determined from the global observation database for the humid  
 133 tropical regions (Köppen class A) (69).

134 Assuming errors  $\varepsilon_i$  are normally distributed, the likelihood function can be written in the following form:

$$p(\delta^2\text{H}_i | \beta_0, \beta_1, \delta^{18}\text{O}_i, \sigma^2) = \frac{1}{\sqrt{2\pi\sigma^2}} \exp\left(-\frac{(\delta^2\text{H}_i - \beta_0 - \beta_1\delta^{18}\text{O}_i)^2}{2\sigma^2}\right) \quad (7)$$

135 The joint posterior distribution of the BLR parameters given the observed isotope data ( $\delta^2\text{H}_i, \delta^{18}\text{O}_i$ ) is:

$$p(\beta_0, \beta_1, \sigma^2 | \text{data}) \propto p(\text{data} | \beta_0, \beta_1, \sigma^2) \times p(\beta_0) \times p(\beta_1) \times p(\sigma^2) \quad (8)$$

136 , where  $p(\text{data} | \beta_0, \beta_1, \sigma^2)$  is the likelihood and  $p(\beta_0)$ ,  $p(\beta_1)$ , and  $p(\sigma^2)$  are the priors.

138 We used a simple algorithm from the Markov chain Monte Carlo (MCMC) methods (78), the Metropolis-  
 139 Hastings (MH) algorithm (79; 80), to estimate the posterior distribution. This algorithm can approximate  
 140 the posterior distribution without the need to compute the normalization constant (81). MH algorithm has  
 141 also proven reliable enough to be used in hydroclimatological problems (e. g. 69; 82; 83; 84; 85; 86; 87; 88).  
 142 MH algorithm can be summarized into several steps as follows:

- 143 1. Initialize the parameters  $\beta_0^{(0)}$ ,  $\beta_1^{(0)}$ , and  $\sigma_0^{2(0)}$  to some initial values.
- 144 2. For iteration  $t = 1$  to  $T$ , where  $T$  is the number of iterations (in this study, we used 10,000 steps  
 145 with the tuning of 2,000 steps which are the "burn in" iterations used to accelerate convergence  
 146 (78; 89)):

147 (a) Calculate the acceptance ratio  $\alpha$ :

$$\alpha = \frac{p(\text{data} | \beta_0, \beta_1, \sigma^{2*}) \times p(\beta_0) \times p(\beta_1) \times p(\sigma^{2*})}{p(\text{data} | \beta_0^{(t-1)}, \beta_1^{(t-1)}, \sigma^{2(t-1)}) \times p(\beta_0^{(t-1)}) \times p(\beta_1^{(t-1)}) \times p(\sigma^{2(t-1)})} \quad (9)$$

148 (b) Generate a uniform random number  $u$  from  $[0, 1]$ .

149 (c) If  $u < \alpha$ , accept the proposed parameters:  $\beta_0^{(t)} = \beta_0, \beta_1^{(t)} = \beta_1, \sigma^{2(t)} = \sigma^{2*}$ . Otherwise,  
 150 keep the previous parameters:  $\beta_0^{(t)} = \beta_0^{(t-1)}, \beta_1^{(t)} = \beta_1^{(t-1)}, \sigma^{2(t)} = \sigma^{2(t-1)}$ .

151 3. After  $T$  iterations, we have samples from the posterior distribution. We use these samples to esti-  
 152 mate the posterior mean, credible intervals, and other properties of the parameters.

153 This study uses a symmetrical Gaussian proposal distribution to simplify computing the acceptance ratio  
 154 (78; 90; 89; 91). We implemented the entire BLR process using the **PyMC3** library within the Python com-  
 155 puting environment (92).

### 156 3 Results and Discussion

157 The number of data points at each isotope observation station can be seen in Figure 2. The three stations  
 158 with the most data collection were the Kemayoran Air Pollution Post in Jakarta (#1), with a total of 47 data  
 159 points, followed by Deli Serdang in North Sumatra (#5) with a total of 46 data points, and in third place is the  
 160 Bengkulu station (#11) which is located on the southwest coast of Sumatra with a total of 43 observations of  
 161 data points. The stations with the fewest number of observations include Tambang (#57), located in Riau,  
 162 and Ranomeeto (#58) in Southeast Sulawesi, each with two data points. Stations with the second-fewest  
 163 number of observations include El Tari (#24) and Kupang in East Nusa Tenggara (#38), Mlati (#49) in Sleman,  
 164 Yogyakarta, Malikusaleh (#53) in North Aceh, Koba (#56) in Bangka Belitung, each of which recorded only  
 165 three data points. The stations with the third-fewest number of observations are Tarempa (#36) in the Riau  
 166 Archipelago, West Seram (#48) in Maluku, and Sorong (#54) in Southwest Papua, each of which only has  
 167 four data points. All stations' average and median data points were 21.968 and 22, respectively. These are  
 168 very small because only about a quarter of the 85 months of observation period had successfully extracted  
 169  $\delta^2\text{H}$  and  $\delta^{18}\text{O}$  values.

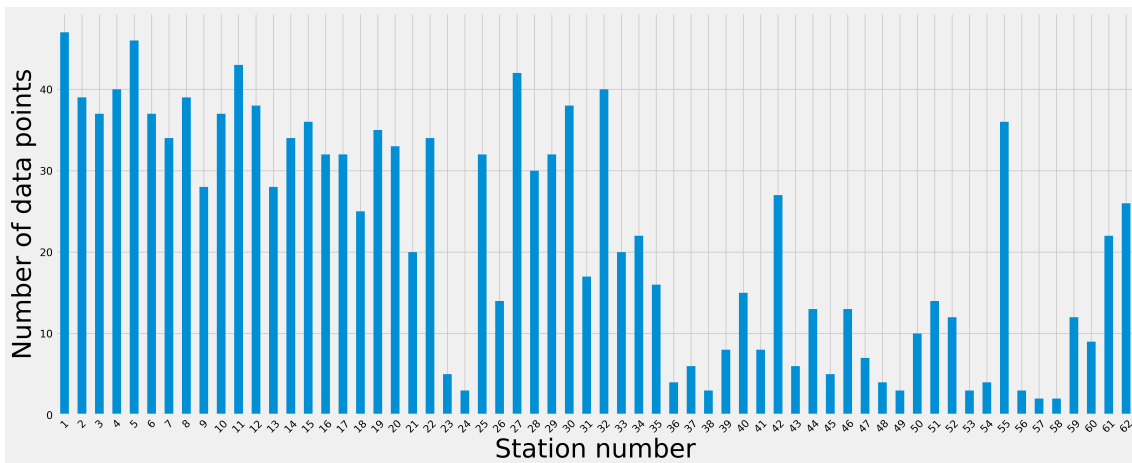


Figure 2: Availability of data points at each isotope station over the IMC collected in this study.

170 Weaknesses in data collection are also found in the need for more coverage of areas outside parts of Suma-  
 171 tra and Java due to limited access to transportation for sending samples. This must be underlined because  
 172 most of the isotope measurements we produced in this study are concentrated in a region with monsoonal  
 173 rainfall classifications (8; 93; 94). In contrast, anti-monsoonal and semi-annual regions are underrepre-  
 174 sented. This is also evident in the less distribution of  $\delta^2\text{H}$  and  $\delta^{18}\text{O}$  values at stations in these two regions,  
 175 as shown in the boxplots in Figure 3.

176 By combining  $\delta^2\text{H}$  and  $\delta^{18}\text{O}$  from all stations, we performed BLR inference, where the results of trace  
 177 plots and the posterior distribution of the linear regression parameters can be seen in Figure 4. There is a  
 178 convergence of all linear regression parameters, which can be visually seen in the trace plots (Figure 4a).  
 179 The posterior distribution of the LMWL parameters that have been calculated using the MH algorithm is  
 180 shown in Figure 4b. The mean and standard deviation of the posterior intercept are 3.506 ‰ and 1.732 ‰,  
 181 respectively. Meanwhile, the mean and standard deviation of the posterior slope are 7.298 ‰ and 0.267  
 182 ‰, respectively. Then, for a  $2\sigma$  credible interval, we can write the LMWL equation as follows:

$$\delta^2\text{H} = 7.298(\pm 0.534)\delta^{18}\text{O} + 3.506(\pm 3.464) \quad (10)$$

183 The two regression coefficients in Equation 10 are shallower when compared to GMWL. This indicates

184 the occurrence of a sub-cloud evaporation process which indicates the occurrence of re-evaporation from  
185 rainwater after falling under the clouds through a tropical convective processes. Visually this can be seen  
186 by shifting the LMWL regression line clockwise when compared to the GMWL (Figure 5). Similar things  
187 were also found in previous studies over the Maritime Continent (95; 96; 26).

## 188 4 Conclusion

189 Based on water isotope observations from 62 stations that we collected from September 2010 to Septem-  
190 ber 2017, we managed to build monthly  $\delta^2\text{H}$ ,  $\delta^{18}\text{O}$ , and d-excess datasets per station and for all IMC, which  
191 are shared openly, accessible, and easily updated on the GitHub repository. We have also performed quality  
192 control on these data by calculating the LMWL using BLR, which is under the range of slopes and intercepts  
193 in previous studies conducted in areas with similar climate types (e. g. 95; 96; 69; 26). The open data we  
194 shared are by far the most complete data over the IMC for stable isotopes of precipitation.

195 There are limitations to this study. One of them is that we should have checked the amount effect. This is  
196 due to the limitation of station precipitation data, which contains many empty data. In the future, a combi-  
197 nation of station data and other high-resolution data sources is needed, such as the Climate Hazards Group  
198 InfraRed Precipitation with Station data (CHIRPS) (97), which can be used to calculate the amount effect.  
199 In addition, this monthly water isotope observation activities over the IMC were stopped in September  
200 2017. This activity should be continued, given the central position of the IMC in the Earth's climate sys-  
201 tem, which is currently undergoing significant changes as a consequence of the unprecedented increase  
202 in anthropogenic radiative forcing. The study of water isotopes in precipitation over the IMC can undoubt-  
203 edly deepen our understanding of anthropogenic and natural attributions in the hydrologic cycle in the  
204 tropics.

## 205 Acknowledgments

206 We are grateful to Michael N. Evans (UMD) for discussing fractionation on precipitation isotopes in the  
207 tropics, which was useful in producing these data. This study was supported by ITB Research, Community  
208 Service and Innovation Program (PPMI-ITB) and Japan Society for the Promotion of Science (JSPS) KAKENHI  
209 (#24510256 and #16H05619). Open-source code and publicly available data can be accessed from: <https://github.com/sandyherho/imc-precip-iso/>.  
210

## 211 References

- 212 [1] S. Yang, T. Zhang, Z. Li, and S. Dong, "Climate variability over the maritime continent and its role in  
213 global climate variation: A review," *Journal of Meteorological Research*, vol. 33, no. 6, pp. 993–1015,  
214 2019.
- 215 [2] P. Xue, P. Malanotte-Rizzoli, J. Wei, and E. A. B. Eltahir, "Coupled ocean-atmosphere modeling  
216 over the Maritime Continent: A review," *Journal of Geophysical Research: Oceans*, vol. 125, no. 6,  
217 p. e2019JC014978, 2020.
- 218 [3] J. S. Godfrey, "The effect of the Indonesian throughflow on ocean circulation and heat exchange with  
219 the atmosphere: A review," *Journal of Geophysical Research: Oceans*, vol. 101, no. C5, pp. 12217–12237,  
220 1996.
- 221 [4] M. Li, A. L. Gordon, L. K. Gruenburg, J. Wei, and S. Yang, "Interannual to decadal response of the  
222 Indonesian throughflow vertical profile to Indo-Pacific forcing," *Geophysical Research Letters*, vol. 47,  
223 no. 11, p. e2020GL087679, 2020.
- 224 [5] S. Makarim, J. Sprintall, Z. Liu, W. Yu, A. Santoso, X.-H. Yan, and R. D. Susanto, "Previously unident-  
225 fied Indonesian Throughflow pathways and freshening in the Indian Ocean during recent decades,"  
226 *Scientific Reports*, vol. 9, no. 1, p. 7364, 2019.
- 227 [6] T. Nagai, T. Hibiya, and F. Syamsudin, "Direct estimates of turbulent mixing in the Indonesian  
228 archipelago and its role in the transformation of the Indonesian throughflow waters," *Geophysical  
229 Research Letters*, vol. 48, no. 6, p. e2020GL091731, 2021.

- 230 [7] A. Santoso, M. H. England, J. B. Kajtar, and W. Cai, "Indonesian Throughflow Variability and Linkage to  
231 ENSO and IOD in an Ensemble of CMIP5 Models," *Journal of Climate*, vol. 35, no. 10, pp. 3161–3178,  
232 2022.
- 233 [8] E. Aldrian and R. D. Susanto, "Identification of three dominant rainfall regions within Indonesia and  
234 their relationship to sea surface temperature," *International Journal of Climatology*, vol. 23, no. 12,  
235 pp. 1435–1452, 2003.
- 236 [9] C.-P. Chang, P. A. Harr, and H.-J. Chen, "Synoptic disturbances over the equatorial South China Sea and  
237 western Maritime Continent during boreal winter," *Monthly Weather Review*, vol. 133, no. 3, pp. 489–  
238 503, 2005.
- 239 [10] C.-P. Chang, Z. Wang, J. McBride, and C.-H. Liu, "Annual cycle of Southeast Asia—Maritime Continent  
240 rainfall and the asymmetric monsoon transition," *Journal of Climate*, vol. 18, no. 2, pp. 287–301, 2005.
- 241 [11] S. C. Peatman, J. Schwendike, C. E. Birch, J. H. Marsham, A. J. Matthews, and G.-Y. Yang, "A local-to-  
242 large scale view of Maritime Continent rainfall: Control by ENSO, MJO, and equatorial waves," *Journal*  
243 *of Climate*, vol. 34, no. 22, pp. 8933–8953, 2021.
- 244 [12] J. Zhu, Z. Guan, and X. Wang, "Variations of Summertime SSTA Independent of ENSO in the Maritime  
245 Continent and Their Possible Impacts on Rainfall in the Asian–Australian Monsoon Region," *Journal of*  
246 *Climate*, vol. 35, no. 24, pp. 7949–7964, 2022.
- 247 [13] C. Chen, S. Sahany, A. F. Moise, X. R. Chua, M. E. Hassim, G. Lim, and V. Prasanna, "ENSO–Rainfall  
248 Teleconnection over the Maritime Continent Enhances and Shifts Eastward under Warming," *Journal*  
249 *of Climate*, vol. 36, no. 14, pp. 4635–4663, 2023.
- 250 [14] C. Gao and G. Li, "Asymmetric effect of enso on the maritime continent precipitation in decaying sum-  
251 mers," *Climate Dynamics*, vol. 61, p. 2839–2852, 2023.
- 252 [15] J. Lu, T. Li, and X. Shen, "Precipitation diurnal cycle over the maritime continent modulated by ENSO,"  
253 *Climate Dynamics*, vol. 61, p. 2547–2564, 2023.
- 254 [16] C. Hu, T. Lian, H.-N. Cheung, S. Qiao, Z. Li, K. Deng, S. Yang, and D. Chen, "Mixed diversity of shifting  
255 IOD and El Niño dominates the location of Maritime Continent autumn drought," *National Science*  
256 *Review*, vol. 7, no. 7, pp. 1150–1153, 2020.
- 257 [17] H.-M. Xiao, M.-H. Lo, and J.-Y. Yu, "The increased frequency of combined El Niño and positive IOD  
258 events since 1965s and its impacts on maritime continent hydroclimates," *Scientific Reports*, vol. 12,  
259 no. 1, p. 7532, 2022.
- 260 [18] M.-S. Ahn, D. Kim, Y.-G. Ham, and S. Park, "Role of Maritime Continent land convection on the mean  
261 state and MJO propagation," *Journal of Climate*, vol. 33, no. 5, pp. 1659–1675, 2020.
- 262 [19] Y. Wei, Z. Pu, and C. Zhang, "Diurnal cycle of precipitation over the Maritime Continent under modula-  
263 tion of MJO: Perspectives from cloud-permitting scale simulations," *Journal of Geophysical Research:*  
264 *Atmospheres*, vol. 125, no. 13, p. e2020JD032529, 2020.
- 265 [20] H. Bai and C. Schumacher, "Topographic influences on diurnally driven MJO rainfall over the Maritime  
266 Continent," *Journal of Geophysical Research: Atmospheres*, vol. 127, no. 6, p. e2021JD035905, 2022.
- 267 [21] S. Abhik, H. H. Hendon, and C. Zhang, "The Indo-Pacific Maritime Continent Barrier Effect on MJO  
268 Prediction," *Journal of Climate*, vol. 36, no. 3, pp. 945–957, 2023.
- 269 [22] J. Hudson and E. Maloney, "The Role of Surface Fluxes in MJO Propagation through the Maritime  
270 Continent," *Journal of Climate*, vol. 36, no. 6, pp. 1633–1652, 2023.
- 271 [23] M. D. Yamanaka, "Physical climatology of Indonesian maritime continent: An outline to comprehend  
272 observational studies," *Atmospheric Research*, vol. 178, pp. 231–259, 2016.
- 273 [24] F. Tritschler, M. Binder, F. Händel, D. Burghardt, P. Dietrich, and R. Liedl, "Collected Rain Water as  
274 Cost-Efficient Source for Aquifer Tracer Testing," *Groundwater*, vol. 58, no. 1, pp. 125–131, 2020.
- 275 [25] S. Valdivielso, E. Vázquez-Suñé, and E. Custodio, "Origin and variability of oxygen and hydrogen iso-  
276 topic composition of precipitation in the Central Andes: A review," *Journal of Hydrology*, vol. 587,  
277 p. 124899, 2020.

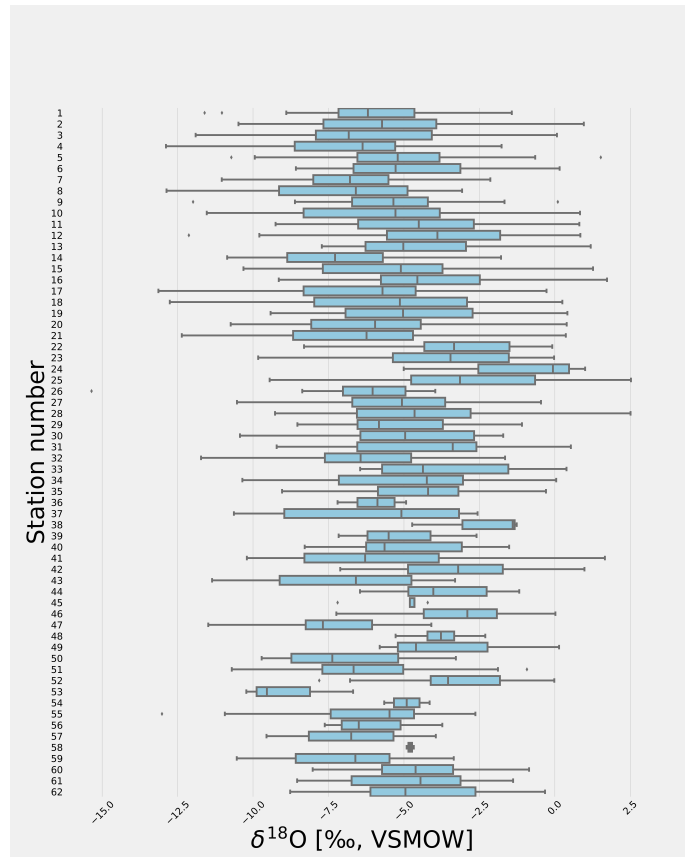


- 278 [26] S. He, D. Jackisch, D. Samanta, P. K. Y. Yi, G. Liu, X. Wang, and N. F. Goodkin, "Understanding tropical  
279 convection through triple oxygen isotopes of precipitation from the maritime continent," *Journal of*  
280 *Geophysical Research: Atmospheres*, vol. 126, no. 4, p. e2020JD033418, 2021.
- 281 [27] F. Malik, S. Butt, and N. Mujahid, "Variation in isotopic composition of precipitation with identification  
282 of vapor source using deuterium excess as tool," *Journal of Radioanalytical and Nuclear Chemistry*,  
283 pp. 1–8, 2022.
- 284 [28] J. Bershaw, "Controls on deuterium excess across Asia," *Geosciences*, vol. 8, no. 7, p. 257, 2018.
- 285 [29] J. Y. Liu, F. P. Zhang, Q. Feng, Y. F. Wei, L. H. Huang, Z. X. Li, S. Nie, and L. Li, "Stable isotopes character-  
286 istics of precipitation over shaanxi-gansu-ningxia and its water vapor sources," *The Journal of Applied*  
287 *Ecology*, vol. 30, no. 7, pp. 2191–2200, 2019.
- 288 [30] C. C. Routson, N. P. McKay, D. S. Kaufman, M. P. Erb, H. Goosse, B. N. Shuman, J. R. Rodysill, and T. Ault,  
289 "Mid-latitude net precipitation decreased with Arctic warming during the Holocene," *Nature*, vol. 568,  
290 no. 7750, pp. 83–87, 2019.
- 291 [31] C. C. Xia, K. Chen, J. Zhou, J. Mei, Y. P. Liu, and G. D. Liu, "Comparison of precipitation stable isotopes  
292 during wet and dry seasons in a subtropical monsoon climate region of China," *Applied Ecology &*  
293 *Environmental Research*, vol. 17, no. 5, 2019.
- 294 [32] C. Xia, G. Liu, K. Chen, Y. Hu, J. Zhou, Y. Liu, and J. Mei, "Stable isotope characteristics for precipitation  
295 events and their responses to moisture and environmental changes during the summer monsoon  
296 period in southwestern china.," *Polish Journal of Environmental Studies*, vol. 29, no. 3, 2020.
- 297 [33] N. Kurita, K. Ichiyanagi, J. Matsumoto, M. D. Yamanaka, and T. Ohata, "The relationship between the  
298 isotopic content of precipitation and the precipitation amount in tropical regions," *Journal of Geo-*  
299 *chemical Exploration*, vol. 102, no. 3, pp. 113–122, 2009.
- 300 [34] N. C. Munksgaard, N. Kurita, R. Sánchez-Murillo, N. Ahmed, L. Araguas, D. L. Balachew, M. I. Bird,  
301 S. Chakraborty, N. K. Chinh, K. M. Cobb, *et al.*, "Data descriptor: Daily observations of stable isotope  
302 ratios of rainfall in the tropics," *Scientific reports*, vol. 9, no. 1, p. 14419, 2019.
- 303 [35] C. Xia, G. Liu, J. Mei, Y. Meng, W. Liu, and Y. Hu, "Characteristics of hydrogen and oxygen stable isotopes  
304 in precipitation and the environmental controls in tropical monsoon climatic zone," *International Jour-*  
305 *nal of Hydrogen Energy*, vol. 44, no. 11, pp. 5417–5427, 2019.
- 306 [36] D. Jackisch, B. X. Yeo, A. D. Switzer, S. He, D. L. M. Cantarero, F. P. Siringan, and N. F. Goodkin, "Pre-  
307 cipitation stable isotopic signatures of tropical cyclones in Metropolitan Manila, Philippines, show  
308 significant negative isotopic excursions," *Natural Hazards and Earth System Sciences*, vol. 22, no. 1,  
309 pp. 213–226, 2022.
- 310 [37] W. Dansgaard, "Stable isotopes in precipitation," *Tellus*, vol. 16, no. 4, pp. 436–468, 1964.
- 311 [38] R. Suwarman, K. Ichiyanagi, M. Tanoue, K. Yoshimura, S. Mori, M. D. Yamanaka, N. Kurita, and F. Syam-  
312 sudin, "The variability of stable isotopes and water origin of precipitation over the Maritime Conti-  
313 nent," *SOLA*, vol. 9, pp. 74–78, 2013.
- 314 [39] H. A. Belgaman, K. Ichiyanagi, M. Tanoue, R. Suwarman, K. Yoshimura, S. Mori, N. Kurita, M. D. Ya-  
315 manaka, and F. Syamsudin, "Intraseasonal variability of  $\delta^{18}\text{O}$  of precipitation over the Indonesian  
316 maritime continent related to the Madden-Julian oscillation," *SOLA*, vol. 12, pp. 192–197, 2016.
- 317 [40] R. Suwarman, K. Ichiyanagi, M. Tanoue, K. Yoshimura, S. Mori, M. D. Yamanaka, F. Syamsudin, and  
318 H. A. Belgaman, "El niño southern oscillation signature in atmospheric water isotopes over maritime  
319 continent during wet season," *Journal of the Meteorological Society of Japan. Ser. II*, vol. 95, no. 1,  
320 pp. 49–66, 2017.
- 321 [41] M. N. Evans, S. E. Tolwinski-Ward, D. M. Thompson, and K. J. Anchukaitis, "Applications of proxy system  
322 modeling in high resolution paleoclimatology," *Quaternary Science Reviews*, vol. 76, pp. 16–28, 2013.
- 323 [42] P. Peng, X. J. Zhang, and J. Chen, "Bias correcting isotope-equipped GCMs outputs to build precipita-  
324 tion oxygen isoscape for eastern China," *Journal of Hydrology*, vol. 589, p. 125153, 2020.
- 325 [43] Y. Nan, Z. He, F. Tian, Z. Wei, and L. Tian, "Can we use precipitation isotope outputs of isotopic general  
326 circulation models to improve hydrological modeling in large mountainous catchments on the Tibetan  
327 Plateau?," *Hydrology and Earth System Sciences*, vol. 25, no. 12, pp. 6151–6172, 2021.

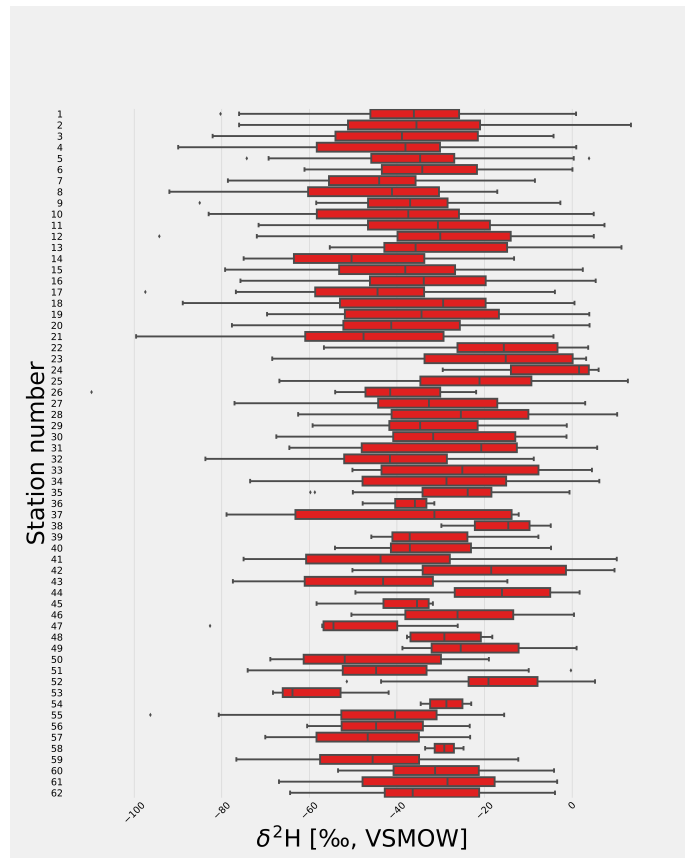
- 328 [44] J. Chen, J. Chen, X. J. Zhang, P. Peng, and C. Risi, "A 148-year precipitation oxygen isoscape for China  
329 generated based on data fusion and bias correction of iGCMs simulations," *Earth System Science Data*  
330 *Discussions*, pp. 1–27, 2022.
- 331 [45] J. Chen, J. Chen, X. J. Zhang, P. Peng, and C. Risi, "A century and a half precipitation oxygen isoscape  
332 for China generated using data fusion and bias correction," *Scientific Data*, vol. 10, no. 1, p. 185, 2023.
- 333 [46] H. A. Belgaman, K. Ichiyanagi, M. Tanoue, and R. Suwarman, "Observational research on stable iso-  
334 topes in precipitation over Indonesian maritime continent," *Nihon Suimon Kagaku Kaishi (Online)*,  
335 vol. 46, no. 1, pp. 7–28, 2016.
- 336 [47] H. A. Belgaman, K. Ichiyanagi, R. Suwarman, M. Tanoue, E. Aldrian, A. I. D. Utami, and S. D. A. Kusuman-  
337 ingtyas, "Characteristics of seasonal precipitation isotope variability in Indonesia," *Hydrological Re-*  
338 *search Letters*, vol. 11, no. 2, pp. 92–98, 2017.
- 339 [48] J. Perkel, "Democratic databases: science on GitHub," *Nature*, vol. 538, no. 7623, pp. 127–128, 2016.
- 340 [49] P. Wessel, J. F. Luis, L. Uieda, R. Scharroo, F. Wobbe, W. H. F. Smith, and D. Tian, "The Generic Mapping  
341 Tools Version 6," *Geochemistry, Geophysics, Geosystems*, vol. 20, no. 11, pp. 5556–5564, 2019.
- 342 [50] L. Uieda, D. Tian, W. J. Leong, W. Schlitzer, M. Grund, M. Jones, Y. Fröhlich, L. Toney, J. Yao, Y. Magen,  
343 J.-H. Tong, K. Materna, A. Belem, T. Newton, A. Anant, M. Ziebarth, J. Quinn, and P. Wessel, "PyGMT: A  
344 Python interface for the Generic Mapping Tools," 2023. Software available from [https://doi.org/  
345 10.5281/zenodo.7772533](https://doi.org/10.5281/zenodo.7772533).
- 346 [51] S. De Graaf, H. B. Vonhof, T. Weissbach, J. A. Wassenburg, E. J. Levy, T. Kluge, and G. H. Haug, "A  
347 comparison of isotope ratio mass spectrometry and cavity ring-down spectroscopy techniques for  
348 isotope analysis of fluid inclusion water," *Rapid Communications in Mass Spectrometry*, vol. 34, no. 16,  
349 p. e8837, 2020.
- 350 [52] S. Maithani and M. Pradhan, "Cavity ring-down spectroscopy and its applications to environmental,  
351 chemical and biomedical systems," *Journal of Chemical Sciences*, vol. 132, pp. 1–19, 2020.
- 352 [53] H. Sagayama, N. M. Racine, T. C. Shriver, and D. A. Schoeller, "Comparison of isotope ratio mass spec-  
353 trometry and cavity ring-down spectroscopy procedures and precision of the doubly labeled water  
354 method in different physiological specimens," *Rapid Communications in Mass Spectrometry*, vol. 35,  
355 no. 21, p. e9188, 2021.
- 356 [54] J. A. Hutchings and B. L. Konecky, "Optimization of a Picarro L2140-i cavity ring-down spectrometer for  
357 routine measurement of triple oxygen isotope ratios in meteoric waters," *Atmospheric Measurement*  
358 *Techniques*, vol. 16, no. 6, pp. 1663–1682, 2023.
- 359 [55] J. Zhang and Z. Xu, "Vacuum extraction of high-salinity water for the determination of oxygen and hy-  
360 drogen isotopic compositions using cavity ring-down spectroscopy," *Microchemical Journal*, vol. 190,  
361 p. 108678, 2023.
- 362 [56] G. M. Hornberger, "New manuscript guidelines for the reporting of stable hydrogen, carbon, and oxy-  
363 gen isotope ratio data," *Water Resources Research*, vol. 31, no. 12, pp. 2895–2895, 1995.
- 364 [57] T. B. Coplen, "Normalization of oxygen and hydrogen isotope data," *Chemical Geology: Isotope Geo-*  
365 *science Section*, vol. 72, no. 4, pp. 293–297, 1988.
- 366 [58] D. Taylor, "Work the shell: analyzing comma-separated values (csv) files," *Linux Journal*, vol. 2015,  
367 no. 260, p. 3, 2015.
- 368 [59] S. Mäs, D. Henzen, L. Bernard, M. Müller, S. Jirka, and I. Senner, "Generic schema descriptions for  
369 comma-separated values files of environmental data," in *The 21th AGILE International Conference on*  
370 *Geographic Information Science*, 2018.
- 371 [60] H. Craig, "Isotopic variations in meteoric waters," *Science*, vol. 133, no. 3465, pp. 1702–1703, 1961.
- 372 [61] L. Merlivat and J. Jouzel, "Global climatic interpretation of the deuterium-oxygen 18 relationship for  
373 precipitation," *Journal of Geophysical Research: Oceans*, vol. 84, no. C8, pp. 5029–5033, 1979.
- 374 [62] S. Pfahl and H. Sodemann, "What controls deuterium excess in global precipitation?," *Climate of the*  
375 *Past*, vol. 10, no. 2, pp. 771–781, 2014.

- 376 [63] R. Sánchez-Murillo, A. M. Durán-Quesada, C. Birkel, G. Esquivel-Hernández, and J. Boll, "Tropical pre-  
377 cipitation anomalies and d-excess evolution during El Niño 2014-16," *Hydrological Processes*, vol. 31,  
378 no. 4, pp. 956–967, 2017.
- 379 [64] K. Yoshikawa, J. Úbeda, P. Masías, W. Pari, F. Apaza, P. Vasquez, B. Ccallata, R. Concha, G. Luna, J. Ipar-  
380 raguirre, *et al.*, "Current thermal state of permafrost in the southern Peruvian Andes and potential  
381 impact from El Niño–Southern Oscillation (ENSO)," *Permafrost and Periglacial Processes*, vol. 31, no. 4,  
382 pp. 598–609, 2020.
- 383 [65] L. Shao, L. Tian, Z. Cai, C. Wang, and Y. Li, "Large-scale atmospheric circulation influences the ice core  
384 d-excess record from the central Tibetan Plateau," *Climate Dynamics*, vol. 57, no. 7-8, pp. 1805–1816,  
385 2021.
- 386 [66] S. Van Der Walt, S. C. Colbert, and G. Varoquaux, "The NumPy array: a structure for efficient numerical  
387 computation," *Computing in science & engineering*, vol. 13, no. 2, pp. 22–30, 2011.
- 388 [67] W. McKinney *et al.*, "pandas: a foundational Python library for data analysis and statistics," *Python for  
389 high performance and scientific computing*, vol. 14, no. 9, pp. 1–9, 2011.
- 390 [68] K. Rozanski, L. Araguás-Araguás, and R. Gonfiantini, "Isotopic patterns in modern global precipitation,"  
391 *Climate change in continental isotopic records*, vol. 78, pp. 1–36, 1993.
- 392 [69] A. L. Putman, R. P. Fiorella, G. J. Bowen, and Z. Cai, "A global perspective on local meteoric water lines:  
393 Meta-analytic insight into fundamental controls and practical constraints," *Water Resources Research*,  
394 vol. 55, no. 8, pp. 6896–6910, 2019.
- 395 [70] L. N. Arellano, S. P. Good, R. Sánchez-Murillo, W. T. Jarvis, D. C. Noone, and C. E. Finkenbiner, "Bayesian  
396 estimates of the mean recharge elevations of water sources in the Central America region using stable  
397 water isotopes," *Journal of Hydrology: Regional Studies*, vol. 32, p. 100739, 2020.
- 398 [71] J. A. Torres-Martínez, A. Mora, P. S. K. Knappett, N. Ornelas-Soto, and J. Mahlknecht, "Tracking nitrate  
399 and sulfate sources in groundwater of an urbanized valley using a multi-tracer approach combined  
400 with a bayesian isotope mixing model," *Water Research*, vol. 182, p. 115962, 2020.
- 401 [72] Q. Zhang, H. Wang, and C. Lu, "Tracing sulfate origin and transformation in an area with multiple  
402 sources of pollution in northern China by using environmental isotopes and Bayesian isotope mixing  
403 model," *Environmental Pollution*, vol. 265, p. 115105, 2020.
- 404 [73] X. Kang, Y. Niu, H. Yu, P. Gou, Q. Hou, X. Lu, and Y. Wu, "Effect of rainfall-runoff process on sources and  
405 transformations of nitrate using a combined approach of dual isotopes, hydrochemical and Bayesian  
406 model in the Dagang River basin," *Science of the Total Environment*, vol. 837, p. 155674, 2022.
- 407 [74] A. Zaryab, H. R. Nassery, K. Knoeller, F. Alijani, and E. Minet, "Determining nitrate pollution sources in  
408 the Kabul Plain aquifer (Afghanistan) using stable isotopes and Bayesian stable isotope mixing model,"  
409 *Science of the Total Environment*, vol. 823, p. 153749, 2022.
- 410 [75] H. Mao, C. Wang, S. Qu, F. Liao, G. Wang, and Z. Shi, "Source and evolution of sulfate in the multi-  
411 layer groundwater system in an abandoned mine—Insight from stable isotopes and Bayesian isotope  
412 mixing model," *Science of the Total Environment*, vol. 859, p. 160368, 2023.
- 413 [76] K. Klauenberg, G. Wübbeler, B. Mickan, P. Harris, and C. Elster, "A tutorial on Bayesian normal linear  
414 regression," *Metrologia*, vol. 52, no. 6, p. 878, 2015.
- 415 [77] M. West, "Outlier models and prior distributions in Bayesian linear regression," *Journal of the Royal  
416 Statistical Society Series B: Statistical Methodology*, vol. 46, no. 3, pp. 431–439, 1984.
- 417 [78] G. L. Jones and Q. Qin, "Markov chain Monte Carlo in practice," *Annual Review of Statistics and Its  
418 Application*, vol. 9, pp. 557–578, 2022.
- 419 [79] N. Metropolis, A. W. Rosenbluth, M. N. Rosenbluth, A. H. Teller, and E. Teller, "Equation of state cal-  
420 culations by fast computing machines," *The Journal of Chemical Physics*, vol. 21, no. 6, pp. 1087–1092,  
421 1953.
- 422 [80] W. K. Hastings, "Monte Carlo sampling methods using Markov chains and their applications,"  
423 *Biometrika*, vol. 57, no. 1, pp. 97–109, 1970.

- 424 [81] S. Chib and E. Greenberg, "Understanding the Metropolis-Hastings Algorithm," *The American Statistician*, vol. 49, no. 4, pp. 327–335, 1995.  
425
- 426 [82] Y. Fan, X. Shi, Q. Duan, and L. Yu, "Towards reliable uncertainty quantification for hydrologic predic-  
427 tions, Part I: Development of a particle copula Metropolis Hastings method," *Journal of Hydrology*,  
428 vol. 612, p. 128163, 2022.
- 429 [83] S. Herho, F. Fajary, and D. Irawan, "On the Statistical Learning Analysis of Rain Gauge Data over the  
430 Natuna Islands," *Indonesian Journal of Statistics and Its Applications*, vol. 6, no. 2, pp. 347–357, 2022.
- 431 [84] S. H. S. Herho, "A Univariate Extreme Value Analysis and Change Point Detection of Monthly Discharge  
432 in Kali Kupang, Central Java, Indonesia," *JOIV: International Journal on Informatics Visualization*, vol. 6,  
433 no. 4, pp. 862–868, 2022.
- 434 [85] S. Sharma and P. P. Mujumdar, "Modeling concurrent hydroclimatic extremes with parametric multi-  
435 variate extreme value models," *Water Resources Research*, vol. 58, no. 2, p. e2021WR031519, 2022.
- 436 [86] R. Vinnarasi and C. T. Dhanya, "Time-varying Intensity-Duration-Frequency relationship through  
437 climate-informed covariates," *Journal of Hydrology*, vol. 604, p. 127178, 2022.
- 438 [87] H. Xu, S. Song, T. Guo, and H. Wang, "Two-stage hybrid model for hydrological series prediction based  
439 on a new method of partitioning datasets," *Journal of Hydrology*, vol. 612, p. 128122, 2022.
- 440 [88] B. Zolghadr-Asli, O. Bozorg-Haddad, M. Enayati, and H. A. Loáiciga, "Sensitivity of non-conditional  
441 climatic variables to climate-change deep uncertainty using Markov Chain Monte Carlo simulation,"  
442 *Scientific Reports*, vol. 12, no. 1, p. 1813, 2022.
- 443 [89] L. F. South, M. Riabiz, O. Teymur, and C. J. Oates, "Postprocessing of MCMC," *Annual Review of Statis-  
444 tics and Its Application*, vol. 9, pp. 529–555, 2022.
- 445 [90] C. Karras, A. Karras, M. Avlonitis, and S. Sioutas, "An overview of mcmc methods: From theory to  
446 applications," in *IFIP International Conference on Artificial Intelligence Applications and Innovations*,  
447 pp. 319–332, Springer, 2022.
- 448 [91] S. Agrawal, D. Vats, K. Łatuszyński, and G. O. Roberts, "Optimal scaling of MCMC beyond Metropolis,"  
449 *Advances in Applied Probability*, vol. 55, no. 2, pp. 492–509, 2023.
- 450 [92] J. Salvatier, T. V. Wiecki, and C. Fonnesbeck, "Probabilistic programming in Python using PyMC3," *PeerJ  
451 Computer Science*, vol. 2, p. e55, 2016.
- 452 [93] Supari, F. Tangang, E. Salimun, E. Aldrian, A. Sopaheluwakan, and L. Juneng, "ENSO modulation of  
453 seasonal rainfall and extremes in Indonesia," *Climate Dynamics*, vol. 51, pp. 2559–2580, 2018.
- 454 [94] T. Ferijal, O. Batelaan, and M. Shanafield, "Spatial and temporal variation in rainy season droughts in  
455 the Indonesian Maritime Continent," *Journal of Hydrology*, vol. 603, p. 126999, 2021.
- 456 [95] S. He, N. F. Goodkin, D. Jackisch, M. R. Ong, and D. Samanta, "Continuous real-time analysis of the  
457 isotopic composition of precipitation during tropical rain events: Insights into tropical convection,"  
458 *Hydrological Processes*, vol. 32, no. 11, pp. 1531–1545, 2018.
- 459 [96] S. He, N. F. Goodkin, N. Kurita, X. Wang, and C. M. Rubin, "Stable isotopes of precipitation during  
460 tropical Sumatra Squalls in Singapore," *Journal of Geophysical Research: Atmospheres*, vol. 123, no. 7,  
461 pp. 3812–3829, 2018.
- 462 [97] C. Funk, P. Peterson, M. Landsfeld, D. Pedreros, J. Verdin, S. Shukla, G. Husak, J. Rowland, L. Harrison,  
463 A. Hoell, *et al.*, "The climate hazards infrared precipitation with stations—a new environmental record  
464 for monitoring extremes," *Scientific data*, vol. 2, no. 1, pp. 1–21, 2015.

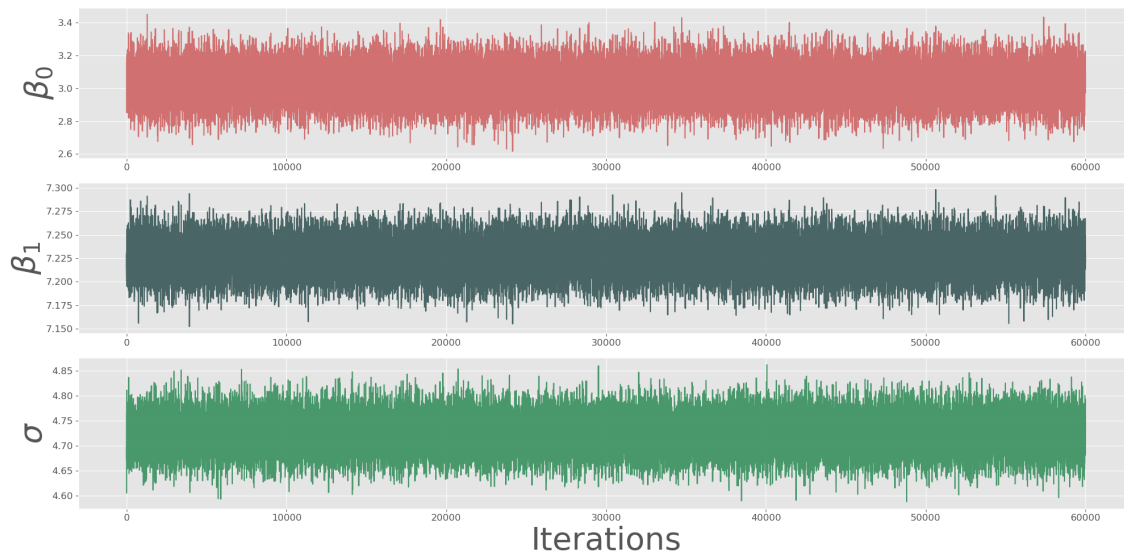


(a)

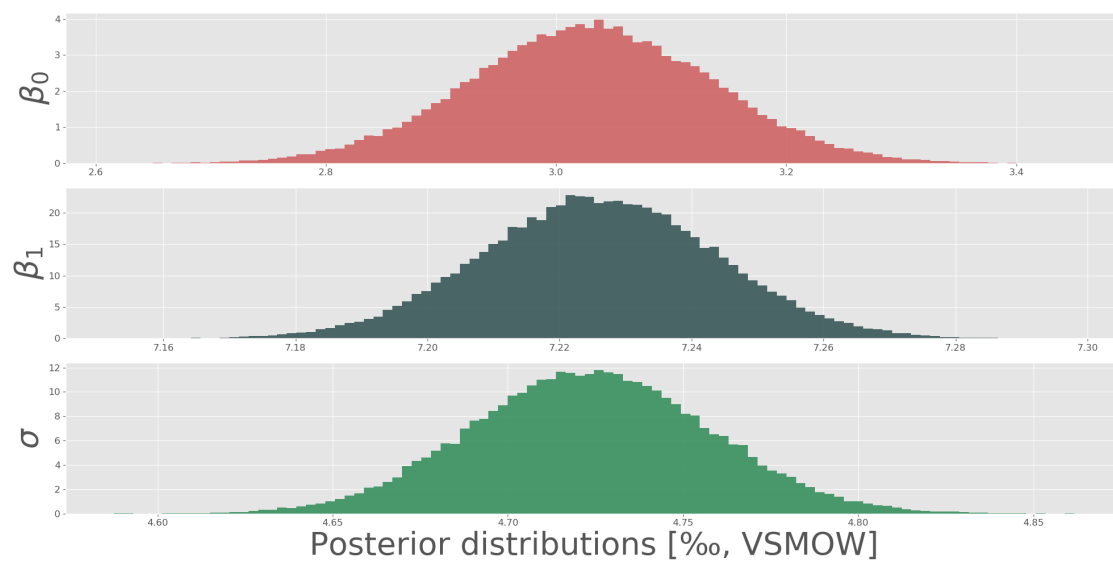


(b)

Figure 3: Box plots of the monthly (a)  $\delta^{18}\text{O}$  and (b)  $\delta^2\text{H}$  recorded by the 62 stations between September 2010 and September 2017.



(a)



(b)

Figure 4: (a) BLR posterior parameter trace plots for the intercept (upper panel), slope (middle panel), and standard deviation (lower panel). (b) Posterior distribution of the three linear regression parameters: intercept (upper panel), slope (middle panel), and standard deviation (lower panel).

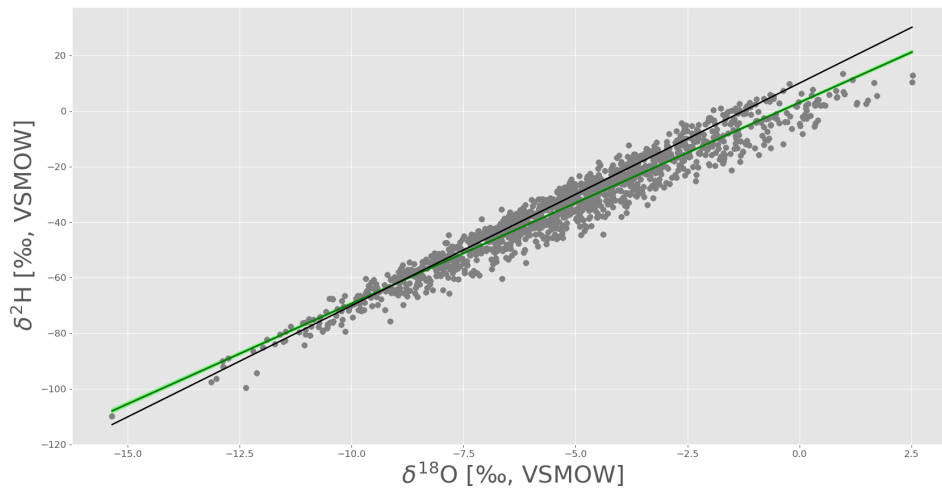


Figure 5: The GMWL (solid black line) compared to the LMWL (the posterior mean shown by a solid green line, light green area shows 95% credible interval obtained from the highest posterior density interval (HPDI)) of all stations over the IMC. Grey dots indicate individual data points.

# imc-precip-iso: Open monthly stable isotope data of precipitation over the Indonesian Maritime Continent

R. Suwarman<sup>1</sup>, S. H. S. Herho<sup>2,3,\*</sup>, H. A. Belgaman<sup>4</sup>, D. E. Irawan<sup>5</sup>, K. Ichiyanagi<sup>6</sup>, I. M. Yosa<sup>1</sup>, A. I. D. Utami<sup>7</sup>, S. Prayogo<sup>8</sup>, and E. Aldrian<sup>4</sup>

<sup>1</sup>Atmospheric Science Research Group, Bandung Institute of Technology (ITB), Bandung, Indonesia

<sup>2</sup>Department of Earth and Planetary Sciences, University of California, Riverside, USA

<sup>3</sup>Department of Geology, University of Maryland, College Park, USA

<sup>4</sup>Research Center for Climate and Atmosphere (PRIMA), National Research and Innovation Agency (BRIN), Bandung, Indonesia

<sup>5</sup>Applied Geology Research Group, Bandung Institute of Technology (ITB), Bandung, Indonesia

<sup>6</sup>Faculty of Advanced Science and Technology, Kumamoto University, Kumamoto, Japan

<sup>7</sup>Indonesian Meteorology, Climatology, and Geophysical Agency (BMKG), Jakarta, Indonesia

<sup>8</sup>Software Engineering Division, Manvis Teknologi Engineering, Bandung, Indonesia

\*Corresponding author: [sandy.herho@email.ucr.edu](mailto:sandy.herho@email.ucr.edu)

## Abstract

Stable isotopes,  $\delta^2\text{H}$ ,  $\delta^{18}\text{O}$ , and d-excess, are valuable tools as natural tracers of diffusion processes and phase changes in the global hydroclimatological cycle. The Indonesian Maritime Continent (IMC) is an archipelago area surrounded by very warm waters which induce convective activities as the primary heat source driving global atmospheric circulation. Given the central role of IMC in this hydroclimatological cycle, comprehensive study and data collection on the stable isotopes of precipitation in this region is crucial.

In this study, we collected monthly stable isotope data from 62 stations spread throughout the Indonesian archipelago from September 2010 to September 2017. We cleaned the data and conducted quality control activities by comparing the Local Meteoric Water Line (LMWL) to previous studies in a similar climatic region. We shared these data openly on our GitHub repository, making them easier to update and interact with users in the future.

## 1 INTRODUCTION

Indonesian Maritime Continent (IMC) comprises a group of islands surrounded by the Indian and Pacific Oceans. The region's climate is influenced by its insular geography and its position near the Equator. Located in the western part of the Indo-Pacific warm pool (IPWP), IMC is a source of latent heat release and deep convection which drives the Hadley and Walker cells, thus playing an essential role in the earth's hydrological cycle (Yang et al., 2019; Xue et al., 2020). IMC is also the only link for warmed surface waters from the Pacific Ocean to the Indian Ocean through the Indonesian Throughflow (ITF), a surface flow component of the global ocean conveyor belt (e. g. Godfrey, 1996; Li et al., 2020; Makarim et al., 2019; Nagai et al., 2021; Santoso et al., 2022).

In general, IMC experiences two seasons, namely the wet and dry seasons, each in boreal winter - spring (November-March/NDJFM) and boreal summer - fall (May - September/MJJAS) (Aldrian and Susanto, 2003; Yang et al., 2019). During the wet season, there is warm sea surface temperature (SST) and heavy precipitation over the IMC, which is brought by the Asian winter monsoon, which is northeasterly to the north of the equator and northwesterly to the south of the equator, the opposite also happens in the dry season (Chang et al., 2005a,b; Yang et al., 2019). Besides the annual cycle, IMC precipitation is influenced by internal global atmosphere-ocean interactions, such as the El Niño Southern Oscillation (ENSO) (e. g.



46 Peatman et al., 2021; Zhu et al., 2022; Chen et al., 2023a; Gao and Li, 2023; Lu et al., 2023) and the Indian  
47 Ocean Dipole mode (IOD) (e. g. Yang et al., 2019; Hu et al., 2020; Peatman et al., 2021; Xiao et al., 2022).  
48 On an intra-annual scale, precipitation over the IMC is also influenced by the Madden-Julian Oscillation  
49 (MJO), which propagates from the Indian Ocean to the Pacific Ocean via IMC (e. g. Ahn et al., 2020; Wei  
50 et al., 2020; Peatman et al., 2021; Bai and Schumacher, 2022; Abhik et al., 2023; Hudson and Maloney,  
51 2023).

52 Given the importance of IMC in understanding the earth's hydroclimatological phenomena (Yamanaka,  
53 2016), investigation of precipitation characteristics is inevitable. One of the characteristics of precipitation  
54 that is important to investigate is the traditional water-stable isotopes of precipitation ( $\delta^{18}\text{O}$  and  $\delta^2\text{H}$ )  
55 which are considered one of the natural tracers of hydrological cycles as a consequence of equilibrium and  
56 kinetic processes during phase transitions and diffusive processes (Tritschler et al., 2020; Valdivielso et al.,  
57 2020; He et al., 2021; Malik et al., 2022). In general, oxygen-18 ( $\delta^{18}\text{O}$ ) and deuterium ( $\delta^2\text{H}$ ) at mid- and  
58 high-latitudes are correlated with temperature (e. g. Bershaw, 2018; Liu et al., 2019; Routson et al., 2019;  
59 Xia et al., 2019b, 2020). However, in tropical regions such as the IMC, these two isotopic compositions  
60 show a negative correlation (e.g. Kurita et al., 2009; Munksgaard et al., 2019; Xia et al., 2019a; Jackisch  
61 et al., 2022) due to a rainout process known as the amount effect (Dansgaard, 1964).  $\delta^{18}\text{O}$  can also be  
62 used as a signature of the water vapour transport process during ENSO and MJO over the IMC (Suwarman  
63 et al., 2013; Belgaman et al., 2016b; Suwarman et al., 2017). Observations of  $\delta^{18}\text{O}$  and  $\delta^2\text{H}$  in the tropics are  
64 also crucial to confirm the sensitivity of proxy precipitation observations in paleoclimatology using proxy  
65 system modelling (PSM), which requires modern precipitation isotope data in the region (Evans et al., 2013).  
66 Modern precipitation isotope observations are also needed to correct calculations performed by isotope-  
67 enabled General Circulation Models (iGCMs) (e. g. Peng et al., 2020; Nan et al., 2021; Chen et al., 2022,  
68 2023b).

69 Until recently, there is not much open and publicly accessible data on traditional precipitation isotope over  
70 the IMC. There are four isotope stations operated by the International Atomic Energy Agency (IAEA) within  
71 the framework of the Global Network of Isotopes in Precipitation (GNIP) program. However, these sta-  
72 tions stopped operating in 2003 and only cover the Java region, except for the Jayapura station in Papua  
73 (Belgaman et al., 2016a). In addition, there were isotope observations conducted by the Institute of Ob-  
74 servational Research for Global Change (IORGC)/Japan Agency for Marine-Earth Science and Technology  
75 (JAMSTEC) conducted at six stations across IMC between 2001 and 2007 (Kurita et al., 2009; Belgaman  
76 et al., 2016a).

77 In this study, we conducted monthly  $\delta^{18}\text{O}$  and  $\delta^2\text{H}$  sampling at 62 observation stations along the IMC  
78 from September 2010 to September 2017. Part of these data (30 stations) have been used in a study by  
79 Belgaman et al. (2017) but has yet to be opened to the public. We opened the  $\delta^{18}\text{O}$  and  $\delta^2\text{H}$  measurements  
80 to the public on our GitHub repository to support democratizing knowledge based on open-source code  
81 and reproducible datasets (Perkel, 2016).

## 82 2 DATA ACQUISITION

83 We conducted field sampling from 62 meteorological and climatological stations owned by the Indonesian  
84 Meteorology, Climatology, and Geophysical Agency (BMKG) throughout the IMC area (Figure 1). To find out  
85 the details of station numbering and their location, see the table on the following URL: [https://github.com/sandyherho/imc-precip-iso/blob/main/output\\_data/sta\\_list.csv](https://github.com/sandyherho/imc-precip-iso/blob/main/output_data/sta_list.csv). We collected these pre-  
86 cipitation samples manually using buckets and then put them into 6 mL glass vials with screw caps. To  
87 prevent secondary evaporation after storage, we discarded samples with a volume of less than 5 mL. We  
88 collected these monthly precipitation samples from September 2010 to September 2017.

90 We measured  $\delta^{18}\text{O}$  and  $\delta^2\text{H}$  using the Picarro<sup>®</sup> L2120-i instrument using the cavity ring-down spectroscopy  
91 technique, which has proven practical and accurate in measuring water isotopes (e. g. De Graaf et al., 2020;  
92 Maithani and Pradhan, 2020; Sagayama et al., 2021; Hutchings and Konecky, 2023; Zhang and Xu, 2023).  
93 We measured the ratio of the abundance of the heavy to light isotopes ( $R$ ), in the context of this study,  
94  $^2\text{H}/^1\text{H}$  and  $^{18}\text{O}/^{16}\text{O}$ , from samples by comparing them to the international standard, namely the Vienna  
95 Standard Mean Ocean Water (VSMOW) (Hornberger, 1995) so that  $\delta$  values were obtained in units per mil  
96 (‰) using the following equation:

$$\delta = \left( \frac{R_{\text{sample}}}{R_{\text{standard}}} - 1 \right) \times 10^3 \quad (1)$$

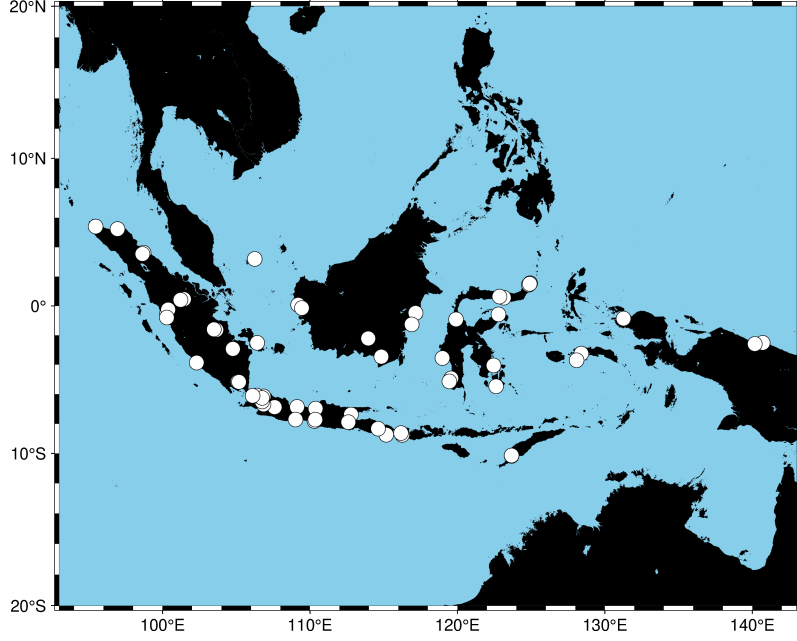


Figure 1: Location of the stations at which monthly samples of precipitation were collected for isotope measurements over the IMC (rendered using PyGMT (Wessel et al., 2019; Uieda et al., 2023)).

97 Due to the limited supply of international standards ( $is$ ), we calibrated the samples ( $x$ ) using three working  
 98 standards ( $ws$ ), Aqua Standard<sup>®</sup>, SLW2 and ICE2, which had been calibrated against VSMOW. This calcula-  
 99 tion process is formulated through the following equation (Coplen, 1988):

$$\delta_{x-is} = \delta_{x-ws} + \delta_{ws-is} + (\delta_{x-ws} \times \delta_{ws-is}) \times 10^{-3} \quad (2)$$

100 Long-term standard errors ( $1\sigma$ ) for these  $\delta^{18}\text{O}$  and  $\delta^2\text{H}$  measurements are  $\pm 0.08 \text{ ‰}$  and  $\pm 0.22 \text{ ‰}$ , re-  
 101 spectively (Belgaman et al., 2017).

102 Microsoft<sup>®</sup> Excel files extracted from the isotope measurement instrument were then converted into a  
 103 text-formatted files, i. e. comma-separated values (CSV) format to make them easier to read by various  
 104 kinds of software without being limited by a paid license (Taylor, 2015; Mäs et al., 2018). These data were  
 105 then splitted into time series for each station and the entire IMC. In addition, we also calculated d-excess  
 106 ( $d$ ), which is defined as the deviation from  $\delta^2\text{H}$  to  $\delta^{18}\text{O}$  according to the definition of the Global Meteoric  
 107 Water Line (GMWL) (Craig, 1961), which can be written as follows:

$$d = \delta^2\text{H} - 8\delta^{18}\text{O} \quad (3)$$

108 Calculation of this d-excess is necessary, given its correlation with the oceanic source of precipitation (Merli-  
 109 vat and Jouzel, 1979; Bershaw, 2018). Globally, this d-excess is a dependent variable of the relative humidity  
 110 of the sea surface (Pfahl and Sodemann, 2014). Using d-excess, we can find the moisture flux anomaly dur-  
 111 ing extreme events, such as ENSO influences in precipitation (e. g. Sánchez-Murillo et al., 2017; Yoshikawa  
 112 et al., 2020; Shao et al., 2021). We did the entire data wrangling process using NumPy (Van Der Walt et al.,  
 113 2011) and pandas (McKinney et al., 2011) libraries in the Python computing environment.

### 114 3 METHOD

115 We performed Local Meteoric Water Line (LMWL) calculations as part of our quality control efforts. It has  
 116 been known since a study conducted by Craig (1961) that there is a linear relationship between  $\delta^2\text{H}$  to  $\delta^{18}\text{O}$   
 117 globally, which can be formulated as follows:

$$\delta^2\text{H} = 8\delta^{18}\text{O} + 10 \quad (4)$$

118 However, local slope variations and intercepts were only discovered after collecting IAEA/GNIP observa-  
 119 tions through the study of Rozanski et al. (1993), better known as LMWL. In this study, it is emphasized

120 that the relationship between the two isotopes is still linear. Variations in the slope may store information  
 121 about the local seasonal climatology (Putman et al., 2019).

122 We used Bayesian Linear Regression (BLR) to determine the relationship between  $\delta^2\text{H}$  and  $\delta^{18}\text{O}$  over the  
 123 IMC. BLR allows better handling of uncertainty in models. This method recognizes that we need perfect  
 124 information about model parameters or data variability. We can represent this uncertainty using a proba-  
 125 bility distribution on the parameters in the Bayesian approach. This approach helps generate more realistic  
 126 and credible parameter estimates and confidence intervals. The BLR approach allows us to incorporate any  
 127 prior knowledge about the model parameters. This is useful when we need more data or want to use ex-  
 128 isting domain knowledge. In this study, we determined the priors for slopes and intercepts from the global  
 129 data compilation for humid tropical regions (Köppen class A) that was done by Putman et al. (2019). Apart  
 130 from single-point estimates (as in "frequentist" linear regression), the BLR gives a full posterior distribution  
 131 of model parameters after looking at the data. This provides richer information about the parameter uncer-  
 132 tainties and allows for more robust modelling of the  $\delta^2\text{H} - \delta^{18}\text{O}$  covariance. Because of these advantages,  
 133 the Bayesian approaches have recently been popular for solving water isotope problems (e. g. Putman  
 134 et al., 2019; Arellano et al., 2020; Torres-Martínez et al., 2020; Zhang et al., 2020; Kang et al., 2022; Zaryab  
 135 et al., 2022; Mao et al., 2023). The full benefits of using BLR can be found in Klauenberg et al. (2015).

136 The simple linear regression model that we used to explain the statistical relationship between  $\delta^2\text{H}$  and  
 137  $\delta^{18}\text{O}$  is illustrated in the following equation:

$$\delta^2\text{H}_i = \beta_0 + \beta_1\delta^{18}\text{O}_i + \varepsilon_i \quad (5)$$

138 , where  $\delta^2\text{H}_i$  and  $\delta^{18}\text{O}_i$  are the observed deuterium and oxygen-18 isotope values for the  $i$ -th data point,  
 139 respectively.  $\beta_0$  and  $\beta_1$  are the unknown regression coefficients (intercept and slope) to be estimated.  
 140  $\varepsilon_i$  is the random error term, assumed to be normally distributed, with mean zero and constant variance  
 141  $\sigma^2$ .

142 BLR estimation started by specifying the prior distributions for the unknown parameters:  $\beta_0$ ,  $\beta_1$ , and  $\sigma^2$ . In  
 143 this study, we assumed normal prior for intercept and slope, and uniform prior for variance (West, 1984):  
 144

$$\begin{cases} \beta_0 \sim \mathcal{N}(m_0, s_0^2) \\ \beta_1 \sim \mathcal{N}(m_1, s_1^2) \\ \sigma^2 \sim U(a, b) \end{cases} \quad (6)$$

145 Parameters  $m_0$ ,  $m_1$ ,  $s_0$ ,  $s_1$ ,  $a$ , and  $b$  were determined from the global observation database for the humid  
 146 tropical regions (Köppen class A) (Putman et al., 2019).

147 Assuming errors  $\varepsilon_i$  are normally distributed, the likelihood function can be written in the following form:

$$p(\delta^2\text{H}_i | \beta_0, \beta_1, \delta^{18}\text{O}_i, \sigma^2) = \frac{1}{\sqrt{2\pi\sigma^2}} \exp\left(-\frac{(\delta^2\text{H}_i - \beta_0 - \beta_1\delta^{18}\text{O}_i)^2}{2\sigma^2}\right) \quad (7)$$

148 The joint posterior distribution of the BLR parameters given the observed isotope data ( $\delta^2\text{H}_i, \delta^{18}\text{O}_i$ ) is:  
 149

$$p(\beta_0, \beta_1, \sigma^2 | \text{data}) \propto p(\text{data} | \beta_0, \beta_1, \sigma^2) \times p(\beta_0) \times p(\beta_1) \times p(\sigma^2) \quad (8)$$

150 , where  $p(\text{data} | \beta_0, \beta_1, \sigma^2)$  is the likelihood and  $p(\beta_0)$ ,  $p(\beta_1)$ , and  $p(\sigma^2)$  are the priors.

151 We used a simple algorithm from the Markov chain Monte Carlo (MCMC) methods (Jones and Qin, 2022),  
 152 the Metropolis-Hastings (MH) algorithm (Metropolis et al., 1953; Hastings, 1970), to estimate the posterior  
 153 distribution. This algorithm can approximate the posterior distribution without the need to compute the  
 154 normalization constant (Chib and Greenberg, 1995). MH algorithm has also proven reliable enough to be  
 155 used in hydroclimatological problems (e. g. Putman et al., 2019; Fan et al., 2022; Herho, 2022; Sharma and  
 156 Mujumdar, 2022; Vinnarasi and Dhanya, 2022; Xu et al., 2022; Zolghadr-Asli et al., 2022). MH algorithm  
 157 can be summarized into several steps as follows:

158 1. Initialize the parameters  $\beta_0^{(0)}$ ,  $\beta_1^{(0)}$ , and  $\sigma_0^{2(0)}$  to some initial values.

159 2. For iteration  $t = 1$  to  $T$ , where  $T$  is the number of iterations (in this study, we used 10,000 steps  
 160 with the tuning of 2,000 steps which are the "burn in" iterations used to accelerate convergence  
 161 (Jones and Qin, 2022; South et al., 2022)):

162 (a) Calculate the acceptance ratio  $\alpha$ :

$$\alpha = \frac{p(\text{data}|\beta_0, \beta_1, \sigma^{2*}) \times p(\beta_0) \times p(\beta_1) \times p(\sigma^{2*})}{p(\text{data}|\beta_0^{(t-1)}, \beta_1^{(t-1)}, \sigma^{2(t-1)}) \times p(\beta_0^{(t-1)}) \times p(\beta_1^{(t-1)}) \times p(\sigma^{2(t-1)})} \quad (9)$$

163 (b) Generate a uniform random number  $u$  from  $[0, 1]$ .

164 (c) If  $u < \alpha$ , accept the proposed parameters:  $\beta_0^{(t)} = \beta_0, \beta_1^{(t)} = \beta_1, \sigma^{2(t)} = \sigma^{2*}$ . Otherwise,  
 165 keep the previous parameters:  $\beta_0^{(t)} = \beta_0^{(t-1)}, \beta_1^{(t)} = \beta_1^{(t-1)}, \sigma^{2(t)} = \sigma^{2(t-1)}$ .

166 3. After  $T$  iterations, we have samples from the posterior distribution. We use these samples to esti-  
 167 mate the posterior mean, credible intervals, and other properties of the parameters.

168 This study uses a symmetrical Gaussian proposal distribution to simplify computing the acceptance ratio  
 169 (Jones and Qin, 2022; Karras et al., 2022; South et al., 2022; Agrawal et al., 2023). We implemented the  
 170 entire BLR process using the PyMC3 library within the Python computing environment (Salvatier et al.,  
 171 2016).

## 172 4 RESULTS and DISCUSSION

173 The number of data points at each isotope observation station can be seen in Figure 2. The three stations  
 174 with the most data collection were the Kemayoran Air Pollution Post in Jakarta (#1), with a total of 47 data  
 175 points, followed by Deli Serdang in North Sumatra (#5) with a total of 46 data points, and in third place is the  
 176 Bengkulu station (#11) which is located on the southwest coast of Sumatra with a total of 43 observations of  
 177 data points. The stations with the fewest number of observations include Tambang (#57), located in Riau,  
 178 and Ranomeeto (#58) in Southeast Sulawesi, each with two data points. Stations with the second-fewest  
 179 number of observations include El Tari (#24) and Kupang in East Nusa Tenggara (#38), Mlati (#49) in Sleman,  
 180 Yogyakarta, Malikusaleh (#53) in North Aceh, Koba (#56) in Bangka Belitung, each of which recorded only  
 181 three data points. The stations with the third-fewest number of observations are Tarempa (#36) in the Riau  
 182 Archipelago, West Seram (#48) in Maluku, and Sorong (#54) in Southwest Papua, each of which only has  
 183 four data points. All stations' average and median data points were 21.968 and 22, respectively. These are  
 184 very small because only about a quarter of the 85 months of observation period had successfully extracted  
 185  $\delta^2\text{H}$  and  $\delta^{18}\text{O}$  values.

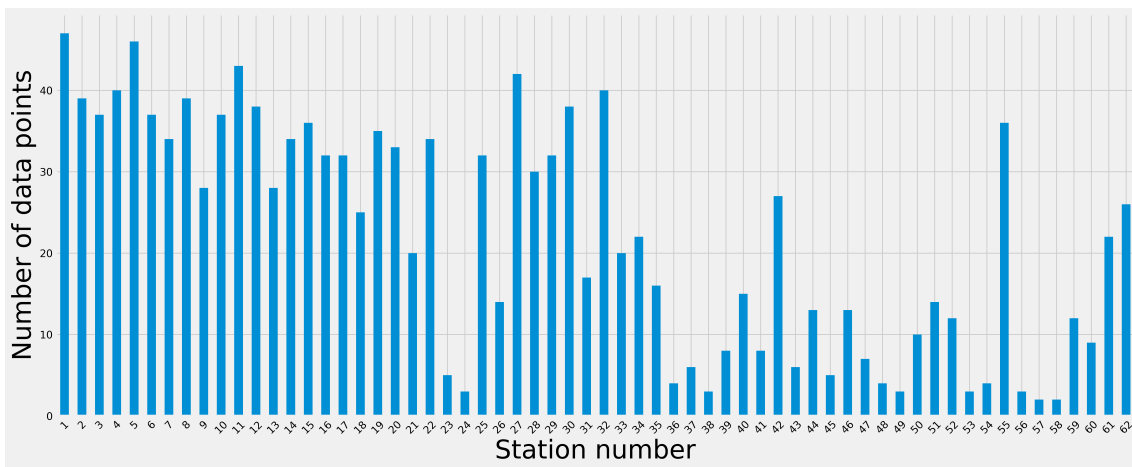


Figure 2: Availability of data points at each isotope station over the IMC collected in this study.

186 Weaknesses in data collection are also found in the need for more coverage of areas outside parts of Suma-  
 187 tra and Java due to limited access to transportation for sending samples. This must be underlined because  
 188 most of the isotope measurements we produced in this study are concentrated in a region with monsoonal

189 rainfall classifications (Aldrian and Susanto, 2003; Supari et al., 2018; Ferijal et al., 2021). In contrast, anti-  
190 monsoonal and semi-annual regions are underrepresented. This is also evident in the less distribution of  
191  $\delta^2\text{H}$  and  $\delta^{18}\text{O}$  values at stations in these two regions, as shown in the boxplots in Figure 3.

192 By combining  $\delta^2\text{H}$  and  $\delta^{18}\text{O}$  from all stations, we performed BLR inference, where the results of trace  
193 plots and the posterior distribution of the linear regression parameters can be seen in Figure 4. There is a  
194 convergence of all linear regression parameters, which can be visually seen in the trace plots (Figure 4a).  
195 The posterior distribution of the LMWL parameters that have been calculated using the MH algorithm is  
196 shown in Figure 4b. The mean and standard deviation of the posterior intercept are 3.506 ‰ and 1.732 ‰,  
197 respectively. Meanwhile, the mean and standard deviation of the posterior slope are 7.298 ‰ and 0.267  
198 ‰, respectively. Then, for a  $2\sigma$  credible interval, we can write the LMWL equation as follows:

$$\delta^2\text{H} = 7.298(\pm 0.534)\delta^{18}\text{O} + 3.506(\pm 3.464) \quad (10)$$

199 The two regression coefficients in Equation 10 are shallower when compared to GMWL. This indicates  
200 the occurrence of a sub-cloud evaporation process which indicates the occurrence of re-evaporation from  
201 rainwater after falling under the clouds through a tropical convective processes. Visually this can be seen  
202 by shifting the LMWL regression line clockwise when compared to the GMWL (Figure 5). Similar things  
203 were also found in previous studies over the Maritime Continent (He et al., 2018a,b, 2021).

## 204 5 CONCLUDING REMARKS

205 Based on water isotope observations from 62 stations that we collected from September 2010 to Septem-  
206 ber 2017, we managed to build monthly  $\delta^2\text{H}$ ,  $\delta^{18}\text{O}$ , and d-excess datasets per station and for all IMC, which  
207 are shared openly, accessible, and easily updated on the GitHub repository. We have also performed quality  
208 control on these data by calculating the LMWL using BLR, which is under the range of slopes and intercepts  
209 in previous studies conducted in areas with similar climate types (e. g. He et al., 2018a,b; Putman et al.,  
210 2019; He et al., 2021). The open data we shared are by far the most complete data over the IMC for stable  
211 isotopes of precipitation.

212 There are limitations to this study. One of them is that we should have checked the amount effect. This  
213 is due to the limitation of station precipitation data, which contains many empty data. In the future, a  
214 combination of station data and other high-resolution data sources is needed, such as the Climate Hazards  
215 Group InfraRed Precipitation with Station data (CHIRPS) (Funk et al., 2015), which can be used to calculate  
216 the amount effect. In addition, this monthly water isotope observation activities over the IMC were stopped  
217 in September 2017. This activity should be continued, given the central position of the IMC in the Earth's  
218 climate system, which is currently undergoing significant changes as a consequence of the unprecedented  
219 increase in anthropogenic radiative forcing. The study of water isotopes in precipitation over the IMC can  
220 undoubtedly deepen our understanding of anthropogenic and natural attributions in the hydrologic cycle  
221 in the tropics.

## 222 FUNDING

223 This study was supported by ITB Research, Community Service and Innovation Program (PPMI-ITB) and  
224 Japan Society for the Promotion of Science (JSPS) KAKENHI (#24510256 and #16H05619).

## 225 DATA AVAILABILITY STATEMENT

226 All relevant code and data are available from this GitHub repository: [https://github.com/sandyherho/  
227 imc-precip-iso](https://github.com/sandyherho/imc-precip-iso).

## 228 CONFLICT OF INTEREST

229 The authors declare there is no conflict.

## References

- 230
- 231 Abhik, S., Hendon, H. H., and Zhang, C. (2023). The Indo-Pacific Maritime Continent Barrier Effect on MJO  
232 Prediction. *Journal of Climate*, 36(3):945–957.
- 233 Agrawal, S., Vats, D., Łatuszyński, K., and Roberts, G. O. (2023). Optimal scaling of MCMC beyond Metropo-  
234 lis. *Advances in Applied Probability*, 55(2):492–509.
- 235 Ahn, M.-S., Kim, D., Ham, Y.-G., and Park, S. (2020). Role of Maritime Continent land convection on the  
236 mean state and MJO propagation. *Journal of Climate*, 33(5):1659–1675.
- 237 Aldrian, E. and Susanto, R. D. (2003). Identification of three dominant rainfall regions within Indonesia and  
238 their relationship to sea surface temperature. *International Journal of Climatology*, 23(12):1435–1452.
- 239 Arellano, L. N., Good, S. P., Sánchez-Murillo, R., Jarvis, W. T., Noone, D. C., and Finkenbiner, C. E. (2020).  
240 Bayesian estimates of the mean recharge elevations of water sources in the Central America region using  
241 stable water isotopes. *Journal of Hydrology: Regional Studies*, 32:100739.
- 242 Bai, H. and Schumacher, C. (2022). Topographic influences on diurnally driven MJO rainfall over the Mar-  
243 itime Continent. *Journal of Geophysical Research: Atmospheres*, 127(6):e2021JD035905.
- 244 Belgaman, H. A., Ichianagi, K., Suwarman, R., Tanoue, M., Aldrian, E., Utami, A. I. D., and Kusumaningtyas,  
245 S. D. A. (2017). Characteristics of seasonal precipitation isotope variability in Indonesia. *Hydrological  
246 Research Letters*, 11(2):92–98.
- 247 Belgaman, H. A., Ichianagi, K., Tanoue, M., and Suwarman, R. (2016a). Observational research on stable  
248 isotopes in precipitation over Indonesian maritime continent. *Nihon Suimon Kagaku Kaishi (Online)*,  
249 46(1):7–28.
- 250 Belgaman, H. A., Ichianagi, K., Tanoue, M., Suwarman, R., Yoshimura, K., Mori, S., Kurita, N., Yamanaka,  
251 M. D., and Syamsudin, F. (2016b). Intraseasonal variability of  $\delta^{18}\text{O}$  of precipitation over the Indonesian  
252 maritime continent related to the Madden–Julian oscillation. *SOLA*, 12:192–197.
- 253 Bershaw, J. (2018). Controls on deuterium excess across Asia. *Geosciences*, 8(7):257.
- 254 Chang, C.-P., Harr, P. A., and Chen, H.-J. (2005a). Synoptic disturbances over the equatorial South China Sea  
255 and western Maritime Continent during boreal winter. *Monthly Weather Review*, 133(3):489–503.
- 256 Chang, C.-P., Wang, Z., McBride, J., and Liu, C.-H. (2005b). Annual cycle of Southeast Asia—Maritime  
257 Continent rainfall and the asymmetric monsoon transition. *Journal of Climate*, 18(2):287–301.
- 258 Chen, C., Sahany, S., Moise, A. F., Chua, X. R., Hassim, M. E., Lim, G., and Prasanna, V. (2023a). ENSO–Rainfall  
259 Teleconnection over the Maritime Continent Enhances and Shifts Eastward under Warming. *Journal of  
260 Climate*, 36(14):4635–4663.
- 261 Chen, J., Chen, J., Zhang, X. J., Peng, P., and Risi, C. (2022). A 148-year precipitation oxygen isoscape for  
262 China generated based on data fusion and bias correction of iGCMs simulations. *Earth System Science  
263 Data Discussions*, pages 1–27.
- 264 Chen, J., Chen, J., Zhang, X. J., Peng, P., and Risi, C. (2023b). A century and a half precipitation oxygen  
265 isoscape for China generated using data fusion and bias correction. *Scientific Data*, 10(1):185.
- 266 Chib, S. and Greenberg, E. (1995). Understanding the Metropolis-Hastings Algorithm. *The American statisti-  
267 cian*, 49(4):327–335.
- 268 Coplen, T. B. (1988). Normalization of oxygen and hydrogen isotope data. *Chemical Geology: Isotope  
269 Geoscience Section*, 72(4):293–297.
- 270 Craig, H. (1961). Isotopic variations in meteoric waters. *Science*, 133(3465):1702–1703.
- 271 Dansgaard, W. (1964). Stable isotopes in precipitation. *Tellus*, 16(4):436–468.
- 272 De Graaf, S., Vonhof, H. B., Weissbach, T., Wassenburg, J. A., Levy, E. J., Kluge, T., and Haug, G. H. (2020).  
273 A comparison of isotope ratio mass spectrometry and cavity ring-down spectroscopy techniques for  
274 isotope analysis of fluid inclusion water. *Rapid Communications in Mass Spectrometry*, 34(16):e8837.
- 275 Evans, M. N., Tolwinski-Ward, S. E., Thompson, D. M., and Anchukaitis, K. J. (2013). Applications of proxy  
276 system modeling in high resolution paleoclimatology. *Quaternary Science Reviews*, 76:16–28.

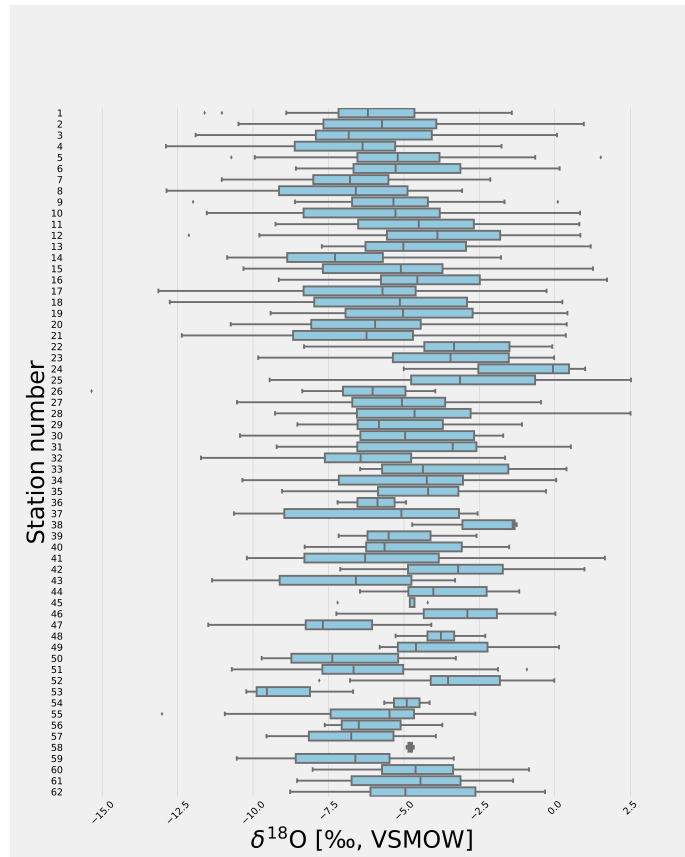
- 277 Fan, Y., Shi, X., Duan, Q., and Yu, L. (2022). Towards reliable uncertainty quantification for hydrologic  
278 predictions, Part I: Development of a particle copula Metropolis Hastings method. *Journal of Hydrology*,  
279 612:128163.
- 280 Ferijal, T., Batelaan, O., and Shanafield, M. (2021). Spatial and temporal variation in rainy season droughts  
281 in the Indonesian Maritime Continent. *Journal of Hydrology*, 603:126999.
- 282 Funk, C., Peterson, P., Landsfeld, M., Pedreros, D., Verdin, J., Shukla, S., Husak, G., Rowland, J., Harrison, L.,  
283 Hoell, A., et al. (2015). The climate hazards infrared precipitation with stations—a new environmental  
284 record for monitoring extremes. *Scientific data*, 2(1):1–21.
- 285 Gao, C. and Li, G. (2023). Asymmetric effect of enso on the maritime continent precipitation in decaying  
286 summers. *Climate Dynamics*, 61:2839–2852.
- 287 Godfrey, J. S. (1996). The effect of the Indonesian throughflow on ocean circulation and heat exchange with  
288 the atmosphere: A review. *Journal of Geophysical Research: Oceans*, 101(C5):12217–12237.
- 289 Hastings, W. K. (1970). Monte Carlo sampling methods using Markov chains and their applications.  
290 *Biometrika*, 57(1):97–109.
- 291 He, S., Goodkin, N. F., Jackisch, D., Ong, M. R., and Samanta, D. (2018a). Continuous real-time analysis of  
292 the isotopic composition of precipitation during tropical rain events: Insights into tropical convection.  
293 *Hydrological Processes*, 32(11):1531–1545.
- 294 He, S., Goodkin, N. F., Kurita, N., Wang, X., and Rubin, C. M. (2018b). Stable isotopes of precipitation during  
295 tropical Sumatra Squalls in Singapore. *Journal of Geophysical Research: Atmospheres*, 123(7):3812–3829.
- 296 He, S., Jackisch, D., Samanta, D., Yi, P. K. Y., Liu, G., Wang, X., and Goodkin, N. F. (2021). Understanding  
297 tropical convection through triple oxygen isotopes of precipitation from the maritime continent. *Journal*  
298 *of Geophysical Research: Atmospheres*, 126(4):e2020JD033418.
- 299 Herho, S. H. S. (2022). A Univariate Extreme Value Analysis and Change Point Detection of Monthly Dis-  
300 charge in Kali Kupang, Central Java, Indonesia. *JOIV: International Journal on Informatics Visualization*,  
301 6(4):862–868.
- 302 Hornberger, G. M. (1995). New manuscript guidelines for the reporting of stable hydrogen, carbon, and  
303 oxygen isotope ratio data. *Water Resources Research*, 31(12):2895–2895.
- 304 Hu, C., Lian, T., Cheung, H.-N., Qiao, S., Li, Z., Deng, K., Yang, S., and Chen, D. (2020). Mixed diversity  
305 of shifting IOD and El Niño dominates the location of Maritime Continent autumn drought. *National*  
306 *Science Review*, 7(7):1150–1153.
- 307 Hudson, J. and Maloney, E. (2023). The Role of Surface Fluxes in MJO Propagation through the Maritime  
308 Continent. *Journal of Climate*, 36(6):1633–1652.
- 309 Hutchings, J. A. and Konecky, B. L. (2023). Optimization of a Picarro L2140-i cavity ring-down spectrometer  
310 for routine measurement of triple oxygen isotope ratios in meteoric waters. *Atmospheric Measurement*  
311 *Techniques*, 16(6):1663–1682.
- 312 Jackisch, D., Yeo, B. X., Switzer, A. D., He, S., Cantarero, D. L. M., Siringan, F. P., and Goodkin, N. F. (2022).  
313 Precipitation stable isotopic signatures of tropical cyclones in Metropolitan Manila, Philippines, show  
314 significant negative isotopic excursions. *Natural Hazards and Earth System Sciences*, 22(1):213–226.
- 315 Jones, G. L. and Qin, Q. (2022). Markov chain Monte Carlo in practice. *Annual Review of Statistics and Its*  
316 *Application*, 9:557–578.
- 317 Kang, X., Niu, Y., Yu, H., Gou, P., Hou, Q., Lu, X., and Wu, Y. (2022). Effect of rainfall-runoff process on  
318 sources and transformations of nitrate using a combined approach of dual isotopes, hydrochemical and  
319 Bayesian model in the Dagang River basin. *Science of the Total Environment*, 837:155674.
- 320 Karras, C., Karras, A., Avlonitis, M., and Sioutas, S. (2022). An overview of mcmc methods: From theory  
321 to applications. In *IFIP International Conference on Artificial Intelligence Applications and Innovations*,  
322 pages 319–332. Springer.
- 323 Klauenberg, K., Wübbeler, G., Mickan, B., Harris, P., and Elster, C. (2015). A tutorial on Bayesian normal  
324 linear regression. *Metrologia*, 52(6):878.

- 325 Kurita, N., Ichiyanagi, K., Matsumoto, J., Yamanaka, M. D., and Ohata, T. (2009). The relationship between  
326 the isotopic content of precipitation and the precipitation amount in tropical regions. *Journal of Geo-*  
327 *chemical Exploration*, 102(3):113–122.
- 328 Li, M., Gordon, A. L., Gruenburg, L. K., Wei, J., and Yang, S. (2020). Interannual to decadal response  
329 of the Indonesian throughflow vertical profile to Indo-Pacific forcing. *Geophysical Research Letters*,  
330 47(11):e2020GL087679.
- 331 Liu, J. Y., Zhang, F. P., Feng, Q., Wei, Y. F., Huang, L. H., Li, Z. X., Nie, S., and Li, L. (2019). Stable isotopes  
332 characteristics of precipitation over Shaanxi-Gansu-Ningxia and its water vapor sources. *The Journal of*  
333 *Applied Ecology*, 30(7):2191–2200.
- 334 Lu, J., Li, T., and Shen, X. (2023). Precipitation diurnal cycle over the maritime continent modulated by  
335 ENSO. *Climate Dynamics*, 61:2547–2564.
- 336 Maithani, S. and Pradhan, M. (2020). Cavity ring-down spectroscopy and its applications to environmental,  
337 chemical and biomedical systems. *Journal of Chemical Sciences*, 132:1–19.
- 338 Makarim, S., Sprintall, J., Liu, Z., Yu, W., Santoso, A., Yan, X.-H., and Susanto, R. D. (2019). Previously uniden-  
339 tified Indonesian Throughflow pathways and freshening in the Indian Ocean during recent decades. *Sci-*  
340 *entific Reports*, 9(1):7364.
- 341 Malik, F., Butt, S., and Mujahid, N. (2022). Variation in isotopic composition of precipitation with identifica-  
342 tion of vapor source using deuterium excess as tool. *Journal of Radioanalytical and Nuclear Chemistry*,  
343 pages 1–8.
- 344 Mao, H., Wang, C., Qu, S., Liao, F., Wang, G., and Shi, Z. (2023). Source and evolution of sulfate in the multi-  
345 layer groundwater system in an abandoned mine—Insight from stable isotopes and Bayesian isotope  
346 mixing model. *Science of the Total Environment*, 859:160368.
- 347 Mäs, S., Henzen, D., Bernard, L., Müller, M., Jirka, S., and Senner, I. (2018). Generic schema descriptions  
348 for comma-separated values files of environmental data. In *The 21th AGILE International Conference on*  
349 *Geographic Information Science*.
- 350 McKinney, W. et al. (2011). pandas: a foundational Python library for data analysis and statistics. *Python*  
351 *for high performance and scientific computing*, 14(9):1–9.
- 352 Merlivat, L. and Jouzel, J. (1979). Global climatic interpretation of the deuterium-oxygen 18 relationship for  
353 precipitation. *Journal of Geophysical Research: Oceans*, 84(C8):5029–5033.
- 354 Metropolis, N., Rosenbluth, A. W., Rosenbluth, M. N., Teller, A. H., and Teller, E. (1953). Equation of state  
355 calculations by fast computing machines. *The Journal of Chemical Physics*, 21(6):1087–1092.
- 356 Munksgaard, N. C., Kurita, N., Sánchez-Murillo, R., Ahmed, N., Araguas, L., Balachew, D. L., Bird, M. I.,  
357 Chakraborty, S., Chinh, N. K., Cobb, K. M., et al. (2019). Data descriptor: Daily observations of stable  
358 isotope ratios of rainfall in the tropics. *Scientific Reports*, 9(1):14419.
- 359 Nagai, T., Hibiya, T., and Syamsudin, F. (2021). Direct estimates of turbulent mixing in the Indonesian  
360 archipelago and its role in the transformation of the Indonesian throughflow waters. *Geophysical Re-*  
361 *search Letters*, 48(6):e2020GL091731.
- 362 Nan, Y., He, Z., Tian, F., Wei, Z., and Tian, L. (2021). Can we use precipitation isotope outputs of isotopic  
363 general circulation models to improve hydrological modeling in large mountainous catchments on the  
364 Tibetan Plateau? *Hydrology and Earth System Sciences*, 25(12):6151–6172.
- 365 Peatman, S. C., Schwendike, J., Birch, C. E., Marsham, J. H., Matthews, A. J., and Yang, G.-Y. (2021). A local-  
366 to-large scale view of Maritime Continent rainfall: Control by ENSO, MJO, and equatorial waves. *Journal*  
367 *of Climate*, 34(22):8933–8953.
- 368 Peng, P., Zhang, X. J., and Chen, J. (2020). Bias correcting isotope-equipped GCMs outputs to build precip-  
369 itation oxygen isoscape for eastern China. *Journal of Hydrology*, 589:125153.
- 370 Perkel, J. (2016). Democratic databases: science on GitHub. *Nature*, 538(7623):127–128.
- 371 Pfahl, S. and Sodemann, H. (2014). What controls deuterium excess in global precipitation? *Climate of the*  
372 *Past*, 10(2):771–781.

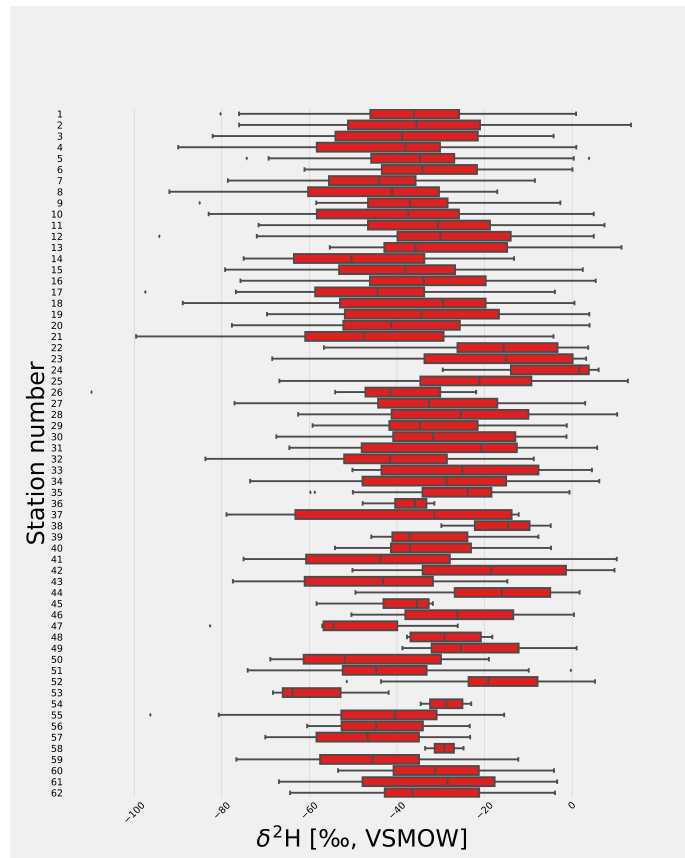


- 373 Putman, A. L., Fiorella, R. P., Bowen, G. J., and Cai, Z. (2019). A global perspective on local meteoric wa-  
374 ter lines: Meta-analytic insight into fundamental controls and practical constraints. *Water Resources*  
375 *Research*, 55(8):6896–6910.
- 376 Routson, C. C., McKay, N. P., Kaufman, D. S., Erb, M. P., Goosse, H., Shuman, B. N., Rodysill, J. R., and Ault,  
377 T. (2019). Mid-latitude net precipitation decreased with Arctic warming during the Holocene. *Nature*,  
378 568(7750):83–87.
- 379 Rozanski, K., Araguás-Araguás, L., and Gonfiantini, R. (1993). Isotopic patterns in modern global precipita-  
380 tion. *Climate change in continental isotopic records*, 78:1–36.
- 381 Sagayama, H., Racine, N. M., Shriver, T. C., and Schoeller, D. A. (2021). Comparison of isotope ratio  
382 mass spectrometry and cavity ring-down spectroscopy procedures and precision of the doubly labeled  
383 water method in different physiological specimens. *Rapid Communications in Mass Spectrometry*,  
384 35(21):e9188.
- 385 Salvatier, J., Wiecki, T. V., and Fonnesbeck, C. (2016). Probabilistic programming in Python using PyMC3.  
386 *PeerJ Computer Science*, 2:e55.
- 387 Sánchez-Murillo, R., Durán-Quesada, A. M., Birkel, C., Esquivel-Hernández, G., and Boll, J. (2017). Trop-  
388 ical precipitation anomalies and d-excess evolution during El Niño 2014-16. *Hydrological Processes*,  
389 31(4):956–967.
- 390 Santoso, A., England, M. H., Kajtar, J. B., and Cai, W. (2022). Indonesian Throughflow Variability and Linkage  
391 to ENSO and IOD in an Ensemble of CMIP5 Models. *Journal of Climate*, 35(10):3161–3178.
- 392 Shao, L., Tian, L., Cai, Z., Wang, C., and Li, Y. (2021). Large-scale atmospheric circulation influences the ice  
393 core d-excess record from the central Tibetan Plateau. *Climate Dynamics*, 57(7-8):1805–1816.
- 394 Sharma, S. and Mujumdar, P. P. (2022). Modeling concurrent hydroclimatic extremes with parametric mul-  
395 tivariate extreme value models. *Water Resources Research*, 58(2):e2021WR031519.
- 396 South, L. F., Riabiz, M., Teymur, O., and Oates, C. J. (2022). Postprocessing of MCMC. *Annual Review of*  
397 *Statistics and Its Application*, 9:529–555.
- 398 Supari, Tangang, F., Salimun, E., Aldrian, E., Sopaheluwakan, A., and Juneng, L. (2018). ENSO modulation  
399 of seasonal rainfall and extremes in Indonesia. *Climate Dynamics*, 51:2559–2580.
- 400 Suwarman, R., Ichiyanagi, K., Tanoue, M., Yoshimura, K., Mori, S., Yamanaka, M. D., Kurita, N., and Syam-  
401 sudin, F. (2013). The variability of stable isotopes and water origin of precipitation over the Maritime  
402 Continent. *SOLA*, 9:74–78.
- 403 Suwarman, R., Ichiyanagi, K., Tanoue, M., Yoshimura, K., Mori, S., Yamanaka, M. D., Syamsudin, F., and Bel-  
404 gaman, H. A. (2017). El niño southern oscillation signature in atmospheric water isotopes over maritime  
405 continent during wet season. *Journal of the Meteorological Society of Japan. Ser. II*, 95(1):49–66.
- 406 Taylor, D. (2015). Work the shell: analyzing comma-separated values (csv) files. *Linux Journal*, 2015(260):3.
- 407 Torres-Martínez, J. A., Mora, A., Knappett, P. S. K., Ornelas-Soto, N., and Mahlknecht, J. (2020). Tracking  
408 nitrate and sulfate sources in groundwater of an urbanized valley using a multi-tracer approach combined  
409 with a bayesian isotope mixing model. *Water Research*, 182:115962.
- 410 Tritschler, F., Binder, M., Händel, F., Burghardt, D., Dietrich, P., and Liedl, R. (2020). Collected Rain Water  
411 as Cost-Efficient Source for Aquifer Tracer Testing. *Groundwater*, 58(1):125–131.
- 412 Uieda, L., Tian, D., Leong, W. J., Schlitzer, W., Grund, M., Jones, M., Fröhlich, Y., Toney, L., Yao, J., Magen,  
413 Y., Tong, J.-H., Materna, K., Belem, A., Newton, T., Anant, A., Ziebarth, M., Quinn, J., and Wessel, P.  
414 (2023). PyGMT: A Python interface for the Generic Mapping Tools. Software available from <https://doi.org/10.5281/zenodo.7772533>.  
415
- 416 Valdivielso, S., Vázquez-Suñé, E., and Custodio, E. (2020). Origin and variability of oxygen and hydrogen  
417 isotopic composition of precipitation in the Central Andes: A review. *Journal of Hydrology*, 587:124899.
- 418 Van Der Walt, S., Colbert, S. C., and Varoquaux, G. (2011). The NumPy array: a structure for efficient nu-  
419 merical computation. *Computing in science & engineering*, 13(2):22–30.
- 420 Vinnarasí, R. and Dhanya, C. T. (2022). Time-varying Intensity-Duration-Frequency relationship through  
421 climate-informed covariates. *Journal of Hydrology*, 604:127178.

- 422 Wei, Y., Pu, Z., and Zhang, C. (2020). Diurnal cycle of precipitation over the Maritime Continent under mod-  
423 ulation of MJO: Perspectives from cloud-permitting scale simulations. *Journal of Geophysical Research:*  
424 *Atmospheres*, 125(13):e2020JD032529.
- 425 Wessel, P., Luis, J. F., Uieda, L., Scharroo, R., Wobbe, F., Smith, W. H. F., and Tian, D. (2019). The Generic  
426 Mapping Tools Version 6. *Geochemistry, Geophysics, Geosystems*, 20(11):5556–5564.
- 427 West, M. (1984). Outlier models and prior distributions in Bayesian linear regression. *Journal of the Royal*  
428 *Statistical Society Series B: Statistical Methodology*, 46(3):431–439.
- 429 Xia, C., Liu, G., Chen, K., Hu, Y., Zhou, J., Liu, Y., and Mei, J. (2020). Stable isotope characteristics for  
430 precipitation events and their responses to moisture and environmental changes during the summer  
431 monsoon period in southwestern china. *Polish Journal of Environmental Studies*, 29(3).
- 432 Xia, C., Liu, G., Mei, J., Meng, Y., Liu, W., and Hu, Y. (2019a). Characteristics of hydrogen and oxygen stable  
433 isotopes in precipitation and the environmental controls in tropical monsoon climatic zone. *International*  
434 *Journal of Hydrogen Energy*, 44(11):5417–5427.
- 435 Xia, C. C., Chen, K., Zhou, J., Mei, J., Liu, Y. P., and Liu, G. D. (2019b). Comparison of precipitation stable  
436 isotopes during wet and dry seasons in a subtropical monsoon climate region of China. *Applied Ecology*  
437 *& Environmental Research*, 17(5).
- 438 Xiao, H.-M., Lo, M.-H., and Yu, J.-Y. (2022). The increased frequency of combined El Niño and positive IOD  
439 events since 1965s and its impacts on maritime continent hydroclimates. *Scientific Reports*, 12(1):7532.
- 440 Xu, H., Song, S., Guo, T., and Wang, H. (2022). Two-stage hybrid model for hydrological series prediction  
441 based on a new method of partitioning datasets. *Journal of Hydrology*, 612:128122.
- 442 Xue, P., Malanotte-Rizzoli, P., Wei, J., and Eltahir, E. A. B. (2020). Coupled ocean-atmosphere modeling over  
443 the Maritime Continent: A review. *Journal of Geophysical Research: Oceans*, 125(6):e2019JC014978.
- 444 Yamanaka, M. D. (2016). Physical climatology of Indonesian maritime continent: An outline to comprehend  
445 observational studies. *Atmospheric Research*, 178:231–259.
- 446 Yang, S., Zhang, T., Li, Z., and Dong, S. (2019). Climate variability over the maritime continent and its role  
447 in global climate variation: A review. *Journal of Meteorological Research*, 33(6):993–1015.
- 448 Yoshikawa, K., Úbeda, J., Masías, P., Pari, W., Apaza, F., Vasquez, P., Ccallata, B., Concha, R., Luna, G., Ipar-  
449 raguirre, J., et al. (2020). Current thermal state of permafrost in the southern Peruvian Andes and poten-  
450 tial impact from El Niño–Southern Oscillation (ENSO). *Permafrost and Periglacial Processes*, 31(4):598–  
451 609.
- 452 Zaryab, A., Nassery, H. R., Knoeller, K., Alijani, F., and Minet, E. (2022). Determining nitrate pollution sources  
453 in the Kabul Plain aquifer (Afghanistan) using stable isotopes and Bayesian stable isotope mixing model.  
454 *Science of the Total Environment*, 823:153749.
- 455 Zhang, J. and Xu, Z. (2023). Vacuum extraction of high-salinity water for the determination of oxygen and hy-  
456 drogen isotopic compositions using cavity ring-down spectroscopy. *Microchemical Journal*, 190:108678.
- 457 Zhang, Q., Wang, H., and Lu, C. (2020). Tracing sulfate origin and transformation in an area with multiple  
458 sources of pollution in northern China by using environmental isotopes and Bayesian isotope mixing  
459 model. *Environmental Pollution*, 265:115105.
- 460 Zhu, J., Guan, Z., and Wang, X. (2022). Variations of Summertime SSTA Independent of ENSO in the Mar-  
461 itime Continent and Their Possible Impacts on Rainfall in the Asian–Australian Monsoon Region. *Journal*  
462 *of Climate*, 35(24):7949–7964.
- 463 Zolghadr-Asli, B., Bozorg-Haddad, O., Enayati, M., and Loáiciga, H. A. (2022). Sensitivity of non-conditional  
464 climatic variables to climate-change deep uncertainty using Markov Chain Monte Carlo simulation. *Sci-*  
465 *entific Reports*, 12(1):1813.

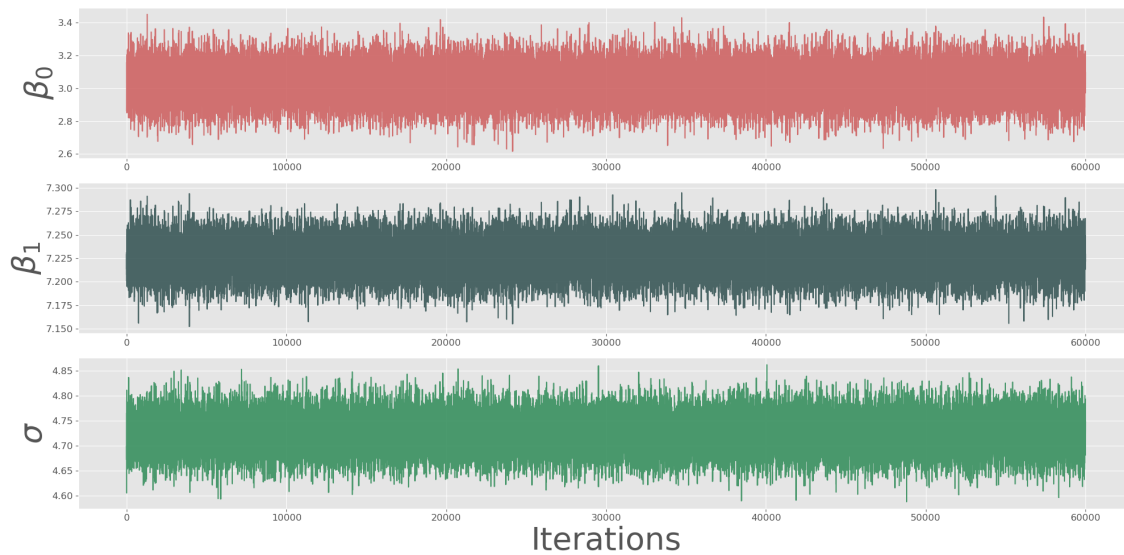


(a)

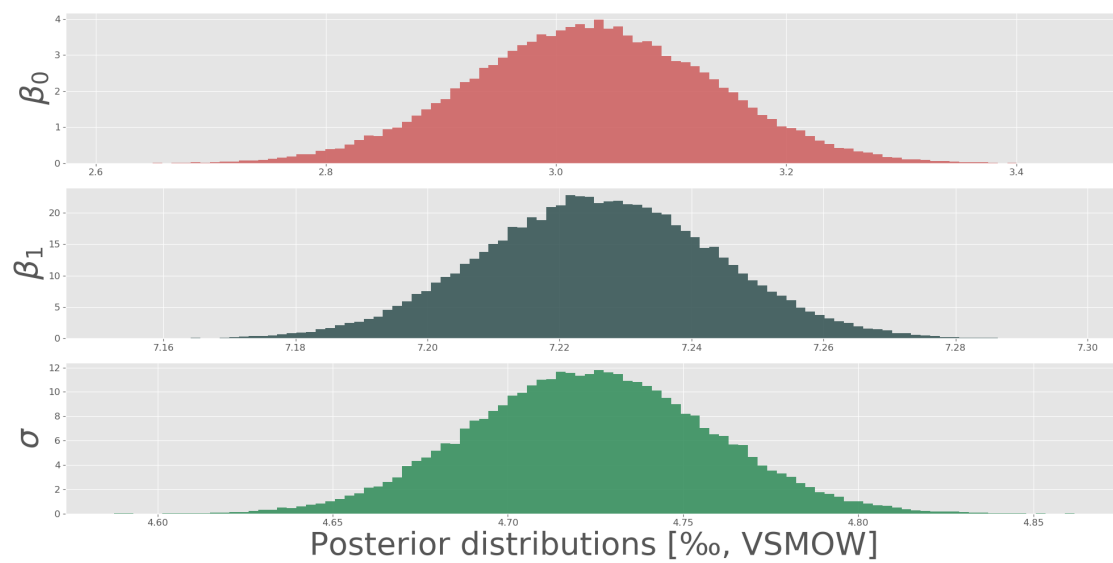


(b)

Figure 3: Box plots of the monthly (a)  $\delta^{18}\text{O}$  and (b)  $\delta^2\text{H}$  recorded by the 62 stations between September 2010 and September 2017.



(a)



(b)

Figure 4: (a) BLR posterior parameter trace plots for the intercept (upper panel), slope (middle panel), and standard deviation (lower panel). (b) Posterior distribution of the three linear regression parameters: intercept (upper panel), slope (middle panel), and standard deviation (lower panel).

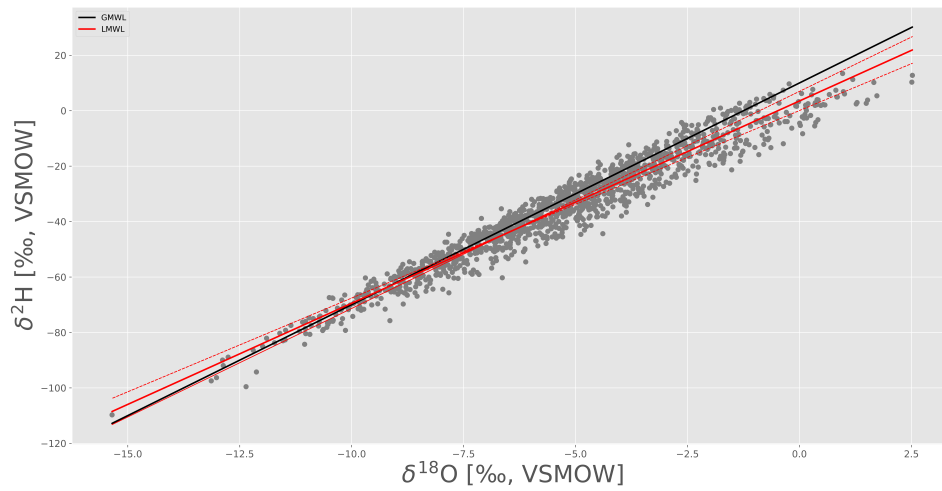


Figure 5: The GMWL (solid black line) compared to the LMWL (the posterior mean shown by a solid red line, area between the dashed red lines shows 95% credible interval obtained from the highest posterior density interval (HPDI)) of all stations over the IMC. Grey dots indicate individual data points.